Computational modelling of long bone fractures fixed with locking plates : how can the risk of non-union/implant failure be reduced?

AUTHOR(S)

Mujtaba Nassiri

CITATION

Nassiri, Mujtaba (2010): Computational modelling of long bone fractures fixed with locking plates : how can the risk of non-union/implant failure be reduced?. Royal College of Surgeons in Ireland. Thesis. https://doi.org/10.25419/rcsi.10801397.v1

DOI

10.25419/rcsi.10801397.v1

RCSI

Computational modelling of long bone fractures fixed with locking plates – how can the risk of non-union/implant failure be reduced?

By

Mujtaba Nassiri

This thesis is submitted to the Royal College of Surgeons in Ireland as the fulfilment of the requirement for the award of the degree of

MCh

Submitted: March 2010

Supervisors:

- Prof. John M. O'Byrne, MCh, FRCS (Tr. & Orth.), Professor of Orthopaedic Surgery, Cappagh National Orthopaedic Hospital.
- Dr. Bryan Mac Donald, B.Eng., M.Sc., Ph.D., DCU.

Table of contents

Declaration

I declare that this thesis, which I submit to RCSI for examination in consideration of the award of MCh, is my own personal effort. Where any of the content presented is the result of input or data from a related collaborative research programme this is duly acknowledged in the text such that it is possible to ascertain how much of the work is my own. I have not already obtained a degree in RCSI or elsewhere on the basis of this work. Furthermore, I took reasonable care to ensure that the work is original, and, to the best of my knowledge, does not breach copyright law, and has not been taken from other sources except where such work has been cited and acknowledged within the text.

Signed : 

RCSI Student Number : 5902321

Date: 10/03/2010

Acknowledgements

I would like to thank Prof. John M. O'Byrne to whom I am greatly indebted for his guidance, encouragement and support during the past 12 months. I also wish to thank Dr. Bryan Mac Donald for his guidance and advice. His expertise in finite element analysis has been instrumental in the completion of this research. Special thanks also goes to Damien Comiskey, Keith Hickey, Beatrice Kelly and all my family and friends who have supported me throughout my studies.

List of Figures

List of abbreviations

AO	Arbeitsgemeinschaft fur Osteosynthesefragen
AP	Antero-Posterior
COAD	Chronic Obstructive Airway Disease
CT	Computed Tomography
DCP	Dynamic Compression Plate
DoE	Design of Experiment
FE	Finite Element
IFM	Interfragmentary Motion
IFS	Interfragmentary Strain
LC DCP	Limited Contact – Dynamic Compression Plate
LCP	Locking Compression Plate
LISS	Less Invasive Stabilisation system
LVDT	Linear Variable Displacement Transducer
PC-Fix	Point Contact Fixator
UTS	Ultimate Tensile Strength

Summary

The Locking Compression Plate (LCP) is part of a new plate generation requiring an adapted surgical technique and new thinking about commonly used concepts of internal fixation using plates. Knowledge of the fixation stability provided by locking compression plates is very limited and further research is necessary to determine how mechanical stability and risk of implant failure can best be controlled. The results of a study based on finite element analysis using locking compression plate for diaphyseal fractures are presented followed by 3 patient specific finite element analysis case studies.

Several factors were shown to influence stability in compression. Axial stiffness was mainly influenced by the working length. On omission of the two innermost screws near the fracture site, axial stiffness decreased by 39%. Construct stability was also affected by the distance from the plate to the bone. Axial stiffness of the construct decreased by increasing the bone-plate distance.

Increasing the post-fixation fracture angle and the fracture translation reduced construct stability, whereas fracture gap had no effect on construct stability when no bone contact occurred during loading.

Stress analysis of the LCP demonstrated that the maximum von Mises stresses were found in the innermost screws at the screw-head junction. Screw stresses decreased significantly with the removal of the two innermost screws.

When the stresses in the plate were isolated, the maximum von Mises stresses were concentrated at the outer edges of the two outermost empty screw holes. Maximum plate stresses also decreased with the removal of the two innermost screws, a pair at a time. Reduction in stresses was more pronounced when the first pair of innermost screws were removed.

Stress concentrations were localized to a point or a specific region of the implant. The majority of stresses were below the yield stress and would not have led to permanent deformation. Despite this, these stress concentrations can indicate where fatigue failure might occur.

Chapter 1 - Introduction

The potential use of computer models to plan and evaluate surgical treatments was first recognised in the 1980s when the term "computer aided surgery" was coined [11]. However, the use of a patient-specific computer-based anatomical model as a planning tool for surgical treatment in a clinical setting is still not widespread.

Hypothesis:

The hypothesis is that current computational modelling techniques, specifically finite element analysis, are capable of predicting the course of healing of fractures fixed using locking plate techniques and that appropriate finite element models will accurately predict complications such as implant failure or non-union and allow for a deeper understanding of the factors influencing these complications.

Background:

Since the first plate osteosynthesis reported in 1886 by Hansmann [32] from Hamburg, plating methods and surgical techniques have changed to ensure the best possible fracture healing.

There have been multiple attempts to improve fixation of conventional plates to compromised bone. These have included the use of cement to improve screw torque. Schuhli nuts [53] and Zespol [48] plates were used in early attempts to convert a conventional plate into a fixed-angle device whereby the plate functions like an "internal fixator." The AO (Arbeitsgemeinschaft fur Osteosynthesefragen) group refined these early attempts and introduced the Point Contact Fixator (PC-Fix) [8] and the Less Invasive Stabilization system (LISS plate) [16, 26]. The clinical successes of these plates led to the introduction of the Locked Compression Plate and the recent proliferation of locked-plate designs by several manufacturers.

Traditionally, plate osteosynthesis employed the principles of rigid fixation (leading to primary bone union without the formation of callus) with stability of the construct enhanced by compressing the plate directly onto bone. This method involves the stripping of periosteum and compression of the plate against the bone, both of which can lead to ischemia and necrosis of bone directly beneath the plate. Locking plates, such as the LCP, provide 'angular stability' at the plate-screw interface, which allows extra-periosteal fixation of the plate to the bone. By preserving periosteal blood supply to the bone it addresses the importance of the biological factors involved in fracture healing. The principles of flexible fixation are employed where the goal is for indirect healing with the formation of callus.

Bearing this in mind, one must be aware of a balance between flexible fixation, which encourages callus formation and promotes the healing process, and an unstable fixation, which leads to non-union and implant failure.

Although the LCP system offers a number of advantages in fracture management, its successful use requires careful pre-operative planning, consideration of biomechanical principles, and the use of the appropriate plate and screws combined with good surgical technique. Failure to address these issues can lead to potential pitfalls in terms of implant breakage or non-union.

Little recommendations exist in the current literature for the control of construct stability or how the risk of implant failure can be reduced for internal fixators such as the LCP.

Finite element analysis is a computational modeling technique that can be used to gain a greater understanding of the mechanics of a problem. Typically this method works by building a geometric model of the problem (in this case the bone – plate construct), applying appropriate material properties and then specifying the "in service" loads (in this case patient weight). The

results of a finite element analysis provide detailed information on the stresses and strains in the model and enable prediction of the factors which may cause the bone-plate construct to fail.

Aims:

1. Finite Element modeling and validation of the structural mechanics of a locking-plate and bone construct.
2. A parametric analysis of the factors that most influence the fixation stiffness and implant stress.
3. To gain an understanding of the factors affecting stability of the fracture fixation with a non-contact locking plate using computational modeling.
4. Study the mechanical factors resulting in non-union with locking plates.
5. Gain an understanding of the principles influencing the mechanical conditions at the fracture site, the control of inter-fragmentary movement and implant failure, namely: gap size, working length (distance between the first two screws on each side of the fracture site), number and position of the screws, distance between the plate and the bone and the material properties.

Chapter 2 - Literature Review

2.1 Introduction

This chapter presents a critical review of the published work in the areas of; biomechanical loading methods, computational modelling of fracture fixation, mechanical factors influencing bone healing and mechanics of implant failure. The fundamental emphasis is on the FE method and how it can be used to simulate a bone-plate construct.

2.2 Experimental studies of fracture fixation implants

2.2.1 Experimental loading methods

The most popular methods of biomechanical testing of bone and implants were found to be four-point bending, compression and torsion testing as bones typically experience a combination of these loads in vivo [3]. Physiological loading was reserved for testing the structural behaviour of specific types of fracture implants [19]. The method of loading was either static or cyclic, depending on the desired output. In static loading, a load is applied very slowly to the construct, which is known as pseudo-static loading. This provides information on elastic stiffness, yield strength and failure strength of the bone implant construct. Cyclic loading on the other hand is applied continuously to a construct, according to a wave function (for example a gait cycle) and allows analysis of implant fatigue or screw loosening [1]. Many experimental tests studied the yield and failure strength of the numerous implants and configurations.

Torsion testing has generally been carried out using an electro mechanical torsion tester. This consists of a torque load cell at one end of the bone-implant construct which records torque. At the other end a torque load actuator is attached, this applies the turning force and measures the angle of rotation [28, 33, 46]. Stoffel et al. [55] devised a more basic method of

edged supports are knife or point edged supports as used by McCartney et al. [40] and Woo et al. [59]. The advantage of knife edged supports is that they tend not to slip as much as round edged supports. They may, however, cause unwanted indentation in the bone sample.

2.2.2 Structural mechanics of internal fixation

One of the most important factors determining fixation stiffness is whether the fixation is load-bearing or load-sharing. If the fixation is load-sharing then the bone and implant share the loads. Load-bearing refers to the presence of a fracture gap or multiple fractures where the bone cannot support the loads, hence the plate must bear the full weight of the patient. In experimental studies, a fracture gap is modelled so that the mechanical properties of the load-bearing implant can be assessed, rather than the load-sharing mechanics of the bone/implant construct [33]. Florin et al. [25], has shown that when the fracture gap is fully compressed, and subjected to bending loads, there is no significant difference in the elastic stiffness between plate fixation methods. Most experimental studies are therefore conducted using a transverse fracture gap so the influence of the implant and its structural attributes can be assessed [28, 33, 37, 38, 46, 57].

In experimental tests, where a fracture gap is present, it was shown that when the inner sets of screws in a locking plate closest to the fracture gap were removed, a reduction in implant compressive (60%) and torsional (30%) rigidity was found [55]. It was also shown that the stiffness of a locking plate also depended on the distance between the plate and the bone, where it has been shown that if the locking plate was raised from 2mm- 6mm from the bone, the construct stiffness reduced by 10-15%, which agrees with the experimental results found by Ahmad et al. [1]. The span between the innermost screws, however, is the greatest factor affecting compressive and torsional rigidity [20, 55] (Fig. 2.2).

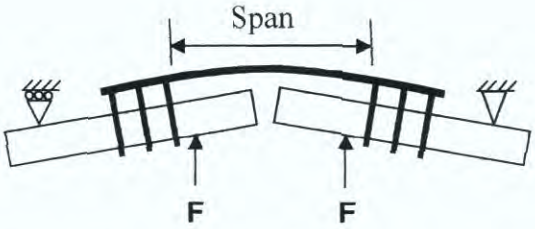

Figure 2.2. Span between innermost screws is most significant factor influencing construct stiffness according to experimental studies.

It should be noted that no experimental studies, as of yet, have included the effect that callus tissue has on structural stiffness. The aforementioned studies were concerned with either modelling a fracture gap, or complete gap closure and compression, where both scenarios yield significantly different stiffness and failure strength outcomes.

2.3 Material properties of metallic implants

The materials in this study are assumed to behave elastically. The elastic stiffness is defined as the ratio between stress and strain (Young's modulus - *E*). The elastic range is assumed to be linear and the yield strength is assumed to be at a 0.2% offset (proof strain) from the modulus of elasticity (*E*) line (Fig. 2.3). The yield strength (σ_y) defines the point where the material begins to deform permanently. Beyond this point the material is said to experience plastic deformation, that is, it will not return to its original form. If the material is continuously loaded past the yield stress, it may reach the ultimate tensile strength (UTS) after which failure will occur.

applying torsion loads using a lever arm with hanging weights attached to one end of the fixation construct. In this model, the distal end is fixed and a lever arm attached to the proximal end and secured in a housed bearing allowing only a single rotational degree of freedom (Fig. 2.1). Weights are added to the lever arm to induce a torsion load. The torque, T, is calculated from the distance, L, from the central axis of the bearing to the point on the lever arm where the weights, W, are hung (T=L*W). A depth gauge is then used to find the displacement of the lever arm which in turn is used to calculate the angle of rotation.

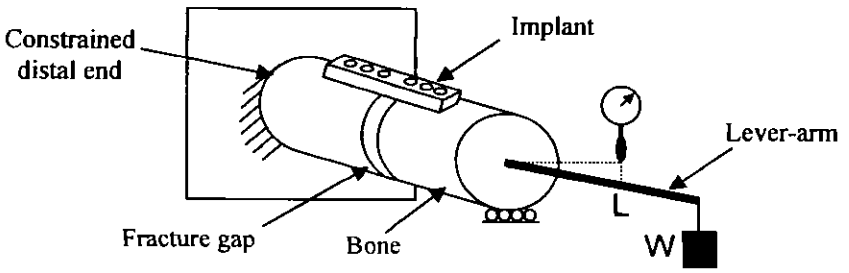

Figure 2.1. Illustration of torque testing rig for implants.

Four-point bending is a biomechanical test method used to assess the flexural or bending stiffness of a fixation construct. Three main types of supports can be used in a bending jig; roller, point or round edged supports. Florin et al. [25] carried out a comparative analysis of four types of plating devices on tubular synthetic bone samples, using four-point bending with roller supports, to asses their biomechanical strength. The ends of the bone substitutes were capped with steel cups with flattened edges to provide the rollers with a path to travel along. Steel pins were located through the steel caps and into bone to prevent rotations. The somewhat excessive measures taken in this study were due to the unsymmetrical double-plated fixation constructs that would inevitably cause rotations under loading. Heiner and Brown [34] carried out a biomechanical study on sawbones composite femur models using round edged supports with a clamp on the distal lower support to prevent axial rotations under four-point bending. An alternative to round

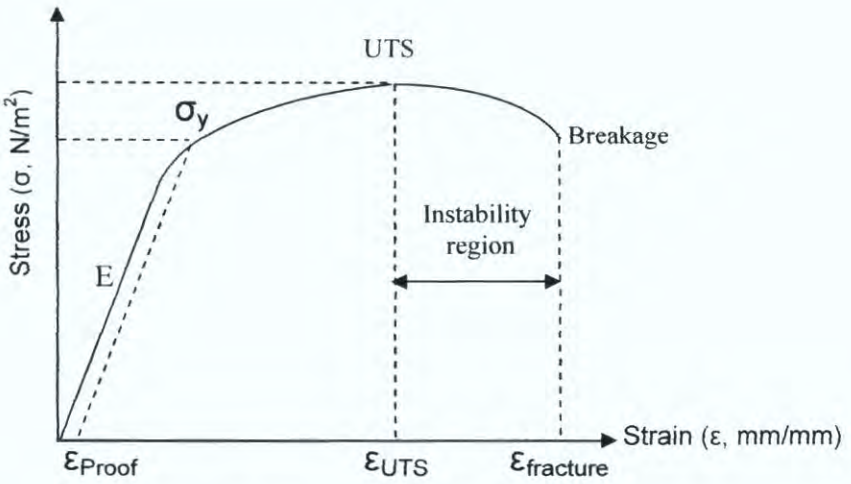

Figure 2.3. Stress strain graph for stainless steel. The instability region is quite often very small and the fracture point can generally be assumed to be at the UTS point for metallic implant materials.

2.3.1 Fatigue

Fatigue is defined as the failure of a component by cyclic or repetitive loading. The process starts with a microscopic crack, called the initiation site, which then widens with each subsequent movement The maximum stress level that a specimen can endure without succumbing to fatigue failure after 10^7 cycles is known as the fatigue limit and is found from S-N tests (stress vs. number of cycles to failure). Theoretically, the specimen could be stressed below the fatigue limit for an infinite number of cycles without failure.

2.4 Mechanics of implant failure

The failure of an implant depends on many factors, such as a fault in the design or manufacture, or by external factors, such as the method of installation, patient co-operation or the rate of fracture healing [50]. According to Sahrma [50], mechanical failure of implants falls into three categories; plastic, brittle and fatigue failure. Plastic failure occurs when the implant experiences stresses greater than the material's yield strength resulting in permanent deformation and clinical failure. Brittle failure is less common and is caused by a defect in design or metallurgy. Fatigue failure occurs by

repetitive loading and consequently surgeons find that there is a 'race' between implant failure and healing of the fracture, where if the bone fails to heal, fatigue failure of the plate is inevitable.

Sharma et al. [50] studied the type and frequency of failures that occurred in 41 patients implanted with either dynamic compression plates or nails between 2001 and 2003. Of these 41failed implants, 30 were plates and 11 were nails (Table 1). From this table it can be seen that breakage is the most common form of implant failure in both plates and nails.

Table 1.1. Sharma et al. (2006)

	Failure mechanism	Anatomy
DCP	19 broken	6 femoral, 3 tibial, 8 humeral and 2 radial
	10 bent	6 femoral, 4 humeral
	1 loosening and infection	Tibia
Nails	5 broken Nails	Femoral
	4 bent Nails	Femoral
	2 broken interlocking nails	Femoral

Screw holes in plates are a common initiation site for fatigue failure, due to the stress concentrations in these locations. The screw holes nearest to the fracture site typically fail through cyclic loading as these screw holes, are most likely to experience greatest stresses where the most mechanical support is required (Fig. 2.4a).

Screw breakage has also been reported in locking plates. El-Sayed et al. [23] successfully fixated fifteen femoral fractures using an experimental locking plate system – A broad DCP with nuts and washers to lock standard screws. Screw failure through bending or breakage, however, occurred in five patients. The screws closest to the fracture site, on either side, were the first to fail, followed by failure of the neighbouring screw(s) (Fig.2.4b).

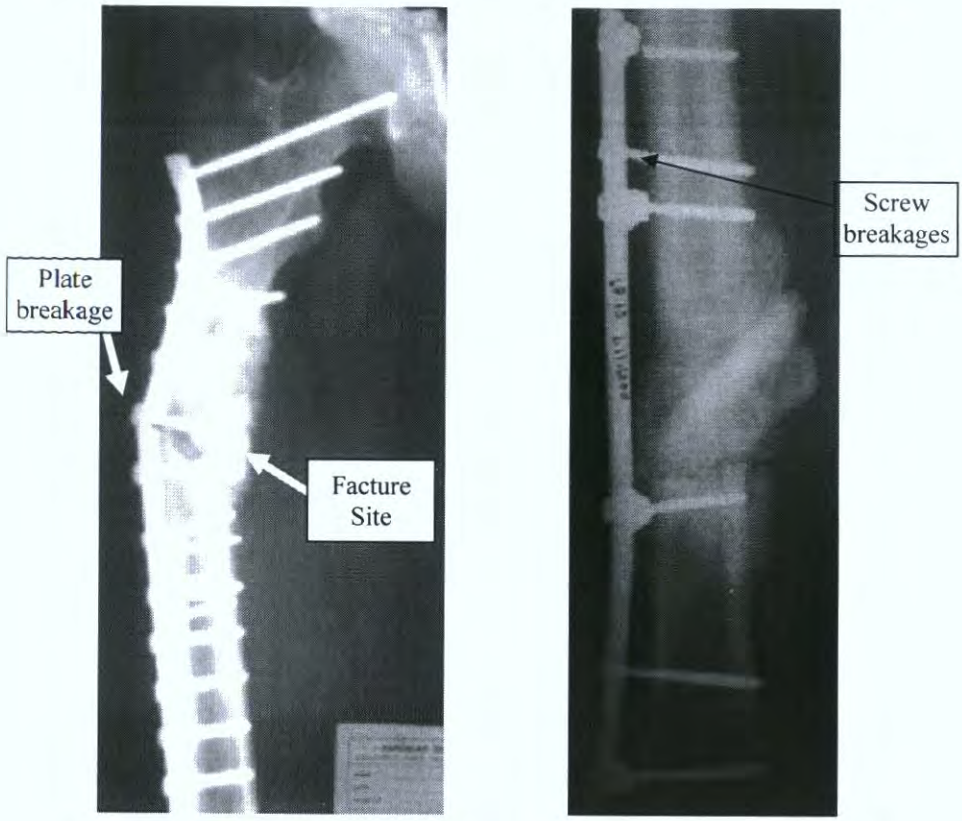

Figure. 2.4. (a) Broken DCP on femur (Sharma et al. 2006) and (b) screw breakage in experimental locking system using a broad DCP with nuts and washers to secure screws (El-Sayed et al., 2001).

2.5 Bone healing

2.5.1 Mechanical properties of a fracture callus

Christel et al. [10] studied the mechanical properties of fracture calluses in rat osteotomies. Christel observed two distinct phases in the healing process, a rubbery-like soft tissue followed by a hard tissue like behaviour. It was found that, up to the first 6 weeks of healing, the callus exhibited low strength, low stiffness and large elongation, which was followed by a harder stiffer material. Between the 6^{th} and 7^{th} week there was a sudden increase in stiffness. Structural stiffness follows a sigmoidal curve (Fig. 2.5a) that highlights the difference between the reparative and remodelling stages of healing. Akkus et al. [2] found a similar sigmoidal relationship between

healing time and callus bending stiffness in rabbits (Fig. 2.5b). Due to the difference in species, there was a more gradual increase in stiffness between the reparative and remodelling phases in comparison to the results found by Christel et al. [10]. This, however, may be due to the method employed in bone fracturing and the size of the fracture gaps themselves.

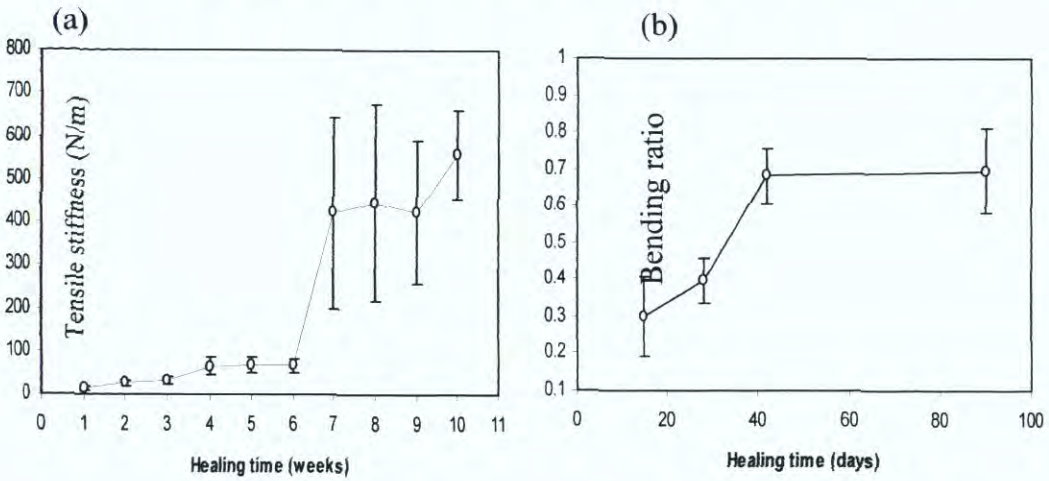

Figure 2.5. (a) Tensile stiffness vs healing time (Christel et al. 1981). The stiffness increased from 35% to 85% of the final value between weeks 6 and 7. (b) Ratio between flexural rigidities vs healing time (Akkus et al. 1998).

Moorcroft et al. [41, 42] studied the visco-elastic characteristics of diaphyseal tibia fracture calluses and how these characteristics changed during the course of healing. In the early stages of healing, the callus absorbs more energy in comparison with the later stages of healing. Moorcroft et al. suggested that the viscous element of the callus reduced with time and the elastic element increased with time. This appears to correspond with the figures above which also show two distinct phases of healing.

2.6 Mechanical factors influencing bone healing

2.6.1 Theories on bone healing and tissue differentiation

The rate or likelihood of a bone to heal successfully is known as the osteogenic potential and is influenced by numerous factors such as hormones, growth factors, age, blood supply and sex. The other factor that influences the osteogenic potential is the level of mechanical stimulus at the fracture site. This has sparked many theories of tissue differentiation based on mechanical stimulus. Pauwels [44] proposed the first theory of mechanical stimulus on tissue differentiation. Pauwels theorised that deviatoric (shear) stresses are the specific stimuli for bone or fibrous connective tissue, whereas hydrostatic (volumetric) stresses control the formation of cartilaginous tissues.

Perren [45] later proposed the "interfragmentary strain theory" which suggests that tissue differentiation is controlled by its resistance to tensile strain. The theory suggests that a tissue cannot form if it experiences strains greater than its rupture strain. Therefore, bone cannot form if the IFS is greater than 2%, endochondral ossification occurs when the IFS is between 2-10% and the formation of granular tissue is present where strain is 100%. Perren therefore suggests that better healing occurs when the strains are low, and since the gap size influences strain, the gap should be large as possible. Importantly, Claes and Heigele [14] dismissed this claim as it defied clinical and logical sense.

2.6.2 Clinical studies of callus healing and mechanical stimulus

Animal studies have been conducted to clarify the influence of mechanical factors on bone healing by quantifying the effect of IFM or IFS on the quality of healing, from a histological and mechanical view-point. These studies typically used idealised fractures in sheep tibiae, such as mid-shaft transversal fractures. Specially designed external fixators have been utilised to induce a specific IFM for a given gap, thus producing a specific IFS.

Goodship and Kenwright [31] quantified the influence of IFS in long bone fractures in sheep tibiae using either a rigid or dynamic unilateral fixator. Strain gauges on the fixator bar were used to quantify the percentage increase in stiffness at a two week interval. It was found that the rate of healing in the dynamic fixator was greater than the rigid fixator (Fig. 2.6a). Goodship and Kenwright induced a constant IFS of 33% using an active system using a pneumatic fixator. A study by Mora and Forriol [43] showed that a passive dynamic fixator which initially allowed 100% IFS, also significantly increased callus stiffness in comparison to the rigidly fixated bones (Fig. 2.6b). The fact that the initial IFS was 100% in one case, (where the cortices could actually completely compress), suggests that dynamic loading at the early stages of healing can significantly influence the rate of increase in callus stiffness.

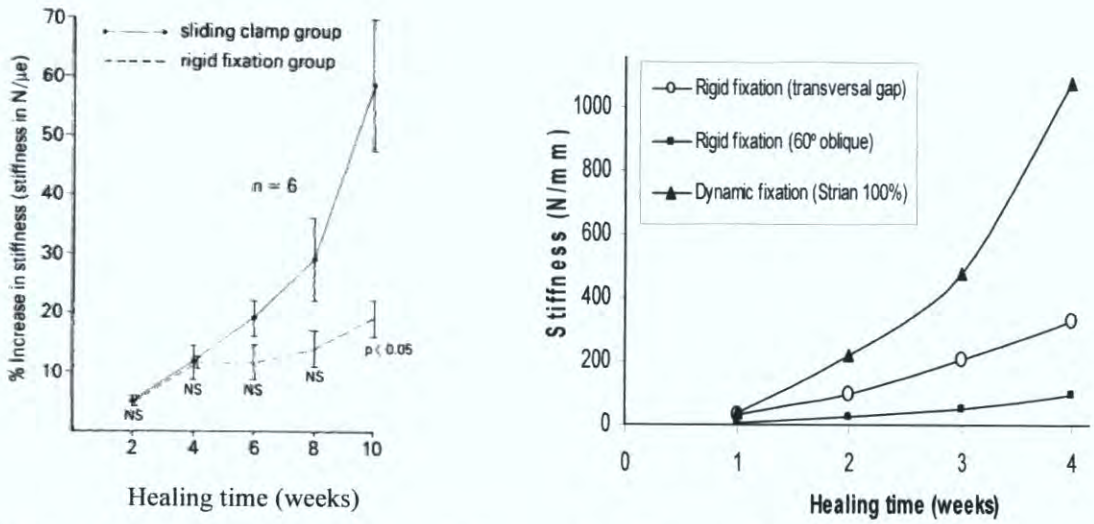

Figure 2.6. (a) Increase in callus stiffness under different fixation methods (Mora and Forriol, 2000) and (b) % increase in stiffness of dynamic and rigid fixation (Goodship and Kenwright, 1985)

In a similar study, Claes et al. [12, 13] used an adjustable external fixator to analyse the affect of fracture gap size and IFS on bone healing in gap osteotomised sheep tibiae. An external fixator which contained a set of springs within telescopic side bars was used to passively allow the required stiffness and level of IFM. The stiffness of the springs could also be adjusted and the maximum stroke could be limited. A linear variable displacement transducer (LVDT) was used to measure the reduction of IFM over the first 8

weeks of healing as the callus evolved. From these results it was concluded that there was no statistically significant difference between the recorded IFMs after the 7th week of healing. A later study by Claes et al. [15] using the same fixator did show, however, that a semi-rigid fixator, which provided more initial IFS in comparison to a rigid fixator did in fact influence the percentage of new bone cells within the fracture fragments.

2.7 Computational modelling of fracture fixation

The earliest 3D numerical studies of a bone and plate fixator were conducted to analyse how the plate and screws affected the stresses and strains experienced by the implant and bone [7, 24, 52]. One-quarter of the FE models were generated using hexahedral elements, so that computational effort could be reduced. Due to the compression plating method, used widely at the time, these FE models assumed that the fracture plane was fully bonded, where healing by direct bone union had occurred. In these studies the bone was simplified into a tube, to represent the mid-diaphysis, and therefore the cancellous bone could be neglected. The material properties were assumed to be linear elastic and isotropic, except in the study by Ferguson et al., where orthotropic material properties from literature were applied to the bone in order to model its anisotropic properties.

Simon et al. [52] carried out the first linear three-dimensional finite element study of a bone-plate-screw construct (Fig. 2.7). Due to computational constraints, frictional contact was neglected in this model by linearly bonding the screw shaft and heads to the bone and plate, respectively. The plate was raised 2mm from the surface of the bone, so that no frictional contact between bone and plate would occur. The quarter symmetric model was then subjected to axial and four-point bending loads. The FE models were subsequently validated by comparing numerically predicted strains to strain-gauge results in experimental models. Simon et al. had shown that the 3D modelling method, when compared with 1D and 2D modelling of plate and bone fixation, yielded the most accurate results. Simon et al. then

demonstrated the capability of the 3D modelling method to determine screw pull-out forces.

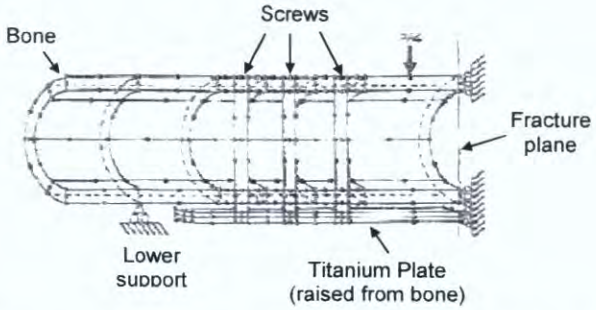

Figure 2.7. Quarter symmetric linear FE model of plate and screw fixation (Adapted from Simon et al., 1977)

Beaupré et al., [6, 7] improved on this study by adding component contact and sliding friction to the bone-plate-screw FE model, for the analysis of stress shielding (Fig. 2.8). Non-linear frictional contact elements were used at the interfaces between the bone and the plate, and between screw heads and plate. It was assumed, however, that the screw shafts were directly bonded to the bone. Screw pretension was also included in this study which was found to induce hydrostatic stress throughout the bone model, which adds to the problem of stress shielding and necrosis under the plate. The use of frictional interfaces also allowed the modelling of slippage between components, which was found to increase strain in the bone.

Figure 2.8. Quarter symmetric FE model of plate and screw fixation (Beaupré et al., 1988).

Ferguson et al., [24] later built a three dimensional finite element model of a plate and screw implantation for the analysis of stress shielding in the bone (Fig. 2.9). Like Beaupré et al., screw pretension and frictional contact were

modelled, and the screw shafts were directly bonded to the bone. The main difference between the studies was that Fergusson et al. analysed the affect of using polymer inserts around the screws and plate, so that a more even stress distribution could be transferred between the highly rigid implants and the less rigid bone. The polymers were assigned stiffness and strengths which were much lower than those of steel and would therefore theoretically reduce stress shielding effects in the bone. Results from the study showed that the inclusion of polymer inserts reduced stress shielding effects in the bone by 14.5%.

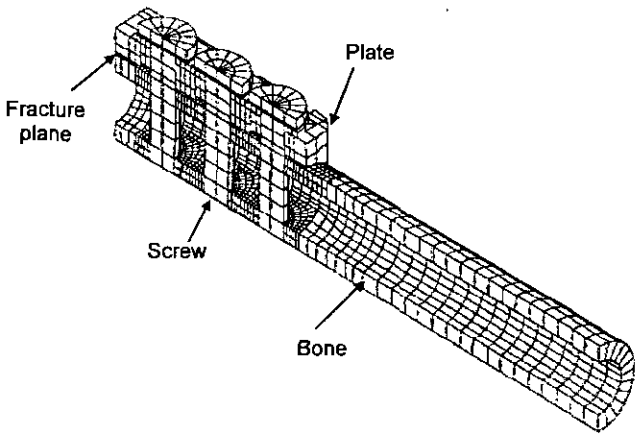

Figure 2.9. Finite element model of bone plate, polymer inserts and screws (Ferguson et al., 1996)

These finite element studies have revealed many possible methods of simplifying models through quarter symmetry, point loads and constraints, linear-elasticity and isotropy. The use of hexahedral (brick-shaped elements) in 3D FE modelling was considered to provide more consistent stress distributions in comparison with tetrahedral elements and with reduced solution time. Frictional contact and pretension was used in compression plating where interface slipping was modelled, however, in the present study, these may be avoided.

Healing by callus formation has become increasingly popular in fracture fixation. Recent FE studies have responded to this by including a fracture

gap between bone fragments [36, 39, 47, 55, 58]. The bone in these FE studies was not required to support loads, the emphasis had shifted from analysing stresses experienced by the bone, to analysing IFM and implant stress. In orthopaedic practice, allowing interfragmentary motion at the fracture site is known as 'dynamisation'. It was suggested that dynamisation could be achieved and controlled by using telescopic external fixators [18]. More recently however, it is understood that interfragmentary motion can be achieved by titration, that is, by reducing the stiffness of the fixator by altering the screw configuration in a plate, or by altering the pins or side bars in an external fixator. This has led to parametric studies of the fixation stiffness of implants.

Lauer et al., [10] conducted a parametric study of an externally fixated bone with a fracture gap using linear 3D finite element beam models. The beam elements were used to represent the pins, bars and bone fragments of the construct, where each beam had an equivalent area moment of inertia. The study was concerned with how the alteration of implant configuration affects interfragmentary strain (IFS) and implant stress. The IFS results were used to quantitatively compare the stiffness's of the different fixation configurations. It was found that the maximum stresses were located at the point where the pins connect to the side bars in all cases. Despite the large number of variables used in this study, there was no systematic design of experiments (DoE) to analyse how the different parameters influenced IFS and implant stress.

Stoffel et al. [55] conducted the only FE study of locking compression. In this case, it was assumed that all the components were linearly bonded and the screw threads could be neglected. Frictional contact was avoided by raising the plate from the bone, mimicking the clinical scenario. Stoffel et al. demonstrated using the FE method that, under compressive loading, the maximum von Mises stresses were experienced by the innermost screw holes in the plate and the innermost screws themselves. He also showed that the plate stress increased by 130% when the innermost screw holes at the fracture site were left unoccupied.

2.7.1 Patient specific FE modelling

Many investigations in biomechanics employ generic FE meshes based on generic patient geometries [51, 56]. However, human anatomical structures have significant variations in geometrical shape and tissue properties among different individuals. Patient specificity is very important in practice for surgical simulation and planning.

Patient specific FE modelling typically involves the conversion of radiographs into CAD models which can be converted into a FE model [27]. There are numerous studies involved with the automatic generation of patient-specific models. Despite this, there has not yet been a breakthrough in patient-specific modelling, whereby a clinician is able to input a CT scan or radiographs and obtain (via the patient specific algorithm) a fully meshed 3D FE model[1].

[1] Key note speech by Prof. Marco Visconti, 'Patient-specific applications of Finite Elements', 2007 Summer Workshop of the European Society of Biomechanics, Trinity College, Dublin, 26-28th August 2007.

Chapter 3 - Methodology

3.1 Introduction

The finite element analysis is to be performed using ANSYS Version 10. The primary objective of this chapter is to undertake a finite element analysis of a transverse fracture fixed with a Locking Compression Plate.

The finite element method is used for finding approximate solutions of partial differential equations. It works by breaking a structure down into many small simple blocks or elements. The behaviour of an individual element can be described with a relatively simple set of equations. The equations describing the behaviours of the individual elements are joined into an extremely large set of equations that describe the behaviour of the whole structure. This large set of simultaneous equations can be solved by a computer and from the solution the behaviour of the individual elements can be calculated. From this, the stress and deflection of all the parts of the structure can be found. The complete solution is then obtained by combining all of the individual solutions for each element together.

3.2 Finite Element Modelling

The first step in the FE modelling procedure is the idealisation and simplification of the problem. Assumptions were made to simplify the geometry, material behaviour, loads and boundary conditions, and contact mechanics.

A detailed list and explanation of the assumptions used in the FE study are given below:

- The screw threads in the FE models were neglected and hence the

geometry of the screw shaft was simplified into a solid cylinder [24, 55]. The inner and outer diameters of a cortical screw's threads are 3.5mm and 4.5mm respectively. In the FE models, however, the thread diameters were disregarded and the shaft diameters of the cortical screws were averaged to 3.5mm. This assumption is made valid by the study by Chao et al. [9] who showed that the relative importance of the threads in comparison to the root diameter shaft is not a significant factor in screw shaft bending stiffness.

- The screw heads were simplified to a solid cylinder, with a diameter of 3.5mm, which provided a perfect fit with screw holes in the plate model.

- The shaft of the femur was assumed to be perfectly tubular and only a pure transverse diaphyseal fracture was modelled.

- The Underside curvature of the locking plate model and ridges were neglected in the FE model and therefore the plate was assumed to be perfectly flat. The staggered screw holes were perfectly aligned (Fig. 3.1).

- The material behaviour was assumed to be linear elastic and isotropic.

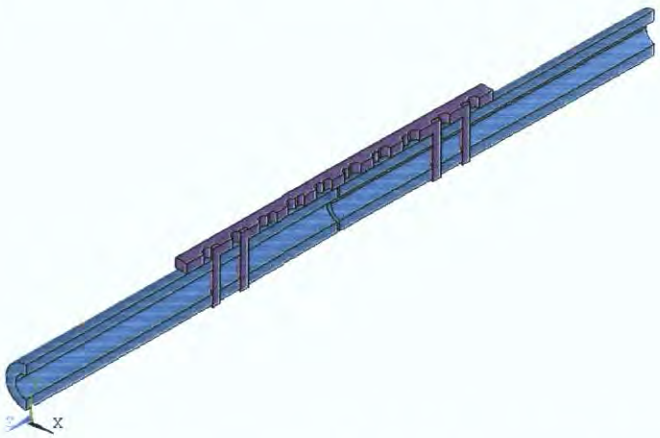

Figure 3.1 Solid model of the locking plate system.

3.2.1 The Locking Compression Plate Model

The finite element model (Fig. 3.2) was created as follows:

- A hollow cylinder was created to represent the bone. It has an outer diameter of 17.8mm, an even wall thickness of 4.15mm, and an inner diameter of 9.5mm. The total length of the cylinder is 281mm; however a 1mm section in the middle of the cylinder is removed to represent the fracture, thus leaving two lengths of 140mm each.

- A solid plate (length 138mm, height 4mm, width 10mm) is created symmetrically on the bone with 10 Combi holes (diameter of holes accommodating dynamic compression screws is 4.5mm and diameter of holes accommodating locking screws is 3.5mm).

- Four 19mm locking screws with a diameter of 3.5mm were created through the two most proximal and the two most distal locking screw holes. The screws are located 11.5mm and 24.5mm from either end of the plate.

- The volumes are then divided up into smaller more manageable volumes in order to concentrate the mesh at areas of high stress concentrations, and also to allow for bonded contact to be setup between the different volumes. Bonded contacts can be created when two volumes beside each other share similar keypoint positions.

- Following bonding, the volumes must be assigned their respective material properties. This bone implant complex is represented using two materials, both of which are assumed to be linear-elastic and isotropic. Labelled "Material 1" represents the bone and is assigned a Young's Modulus of 600 MPa and a Poisson Ration of 0.33. The plate

and the screws are represented by steel, which has a Young's Modulus of 200GPa and a Poisson Ration of 0.27.

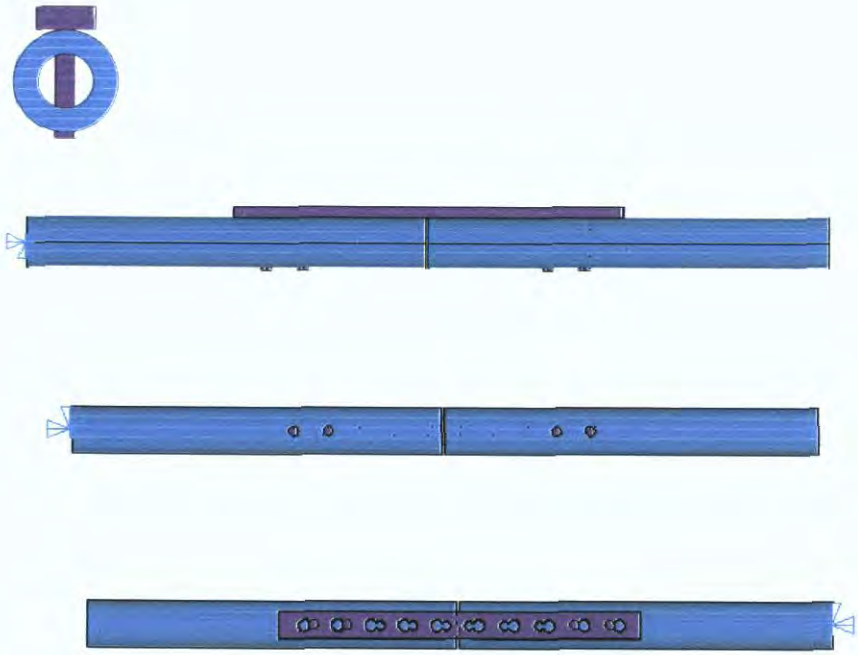

Figure 3.2 Four views of the finite element model

3.2.2 Element Type and Meshing

Following the creation of the model geometry, contact between components and material properties, the next step is to divide the model up into a number of small blocks, or elements, know as the discretisation of the model. The type of element chosen has a significant bearing on the results and it is chosen based chiefly on the shape of the model and also on the loading method and desired results from analysis.

For this model a basic linear pyramid element called (the SOLID 92) is chosen. This element is used for the 3-D modelling of solid structures i.e. they are pyramid elements used to mesh volumes in ANSYS.

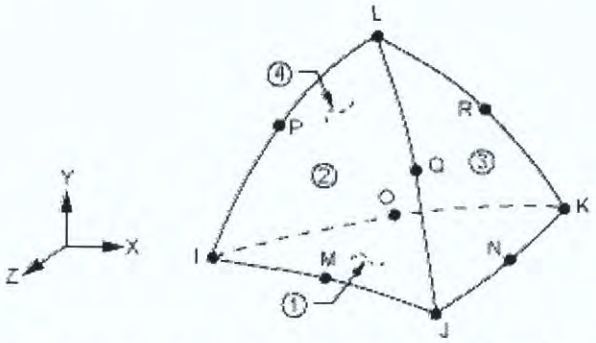

Figure 3.3 10-nodes tetrahedral element (ANSYS SOLID 92). Adapted from the help menu of ANSYS (Version 10) software.

The SOLID 92 element (Fig 3.3.) is defined by ten nodes having three degrees of freedom at each node: translations in the nodal x, y and z directions. The capabilities of the element include analysis of plasticity, creep, swelling, stress stiffening, large deflection, and large strain capabilities.

3.2.3. Axial Compressive Loading

Only axial loading was considered in this study as this is the dominant loading scenario in weight-bearing bones such as the femur and tibia. The application of the axial compressive load is simulated in ANSYS. The axial load is simulated by fixing the distal end of the model and applying a force (400 N) through the bone at the proximal end. This is achieved by selecting only the nodes at the extreme distal end of the bone and constraining them in all degrees of freedom. The nodes at the proximal end of the bone are selected and negative forces in the z–direction are applied to the nodes to simulate the compressive loading situation (fig 3.4.)

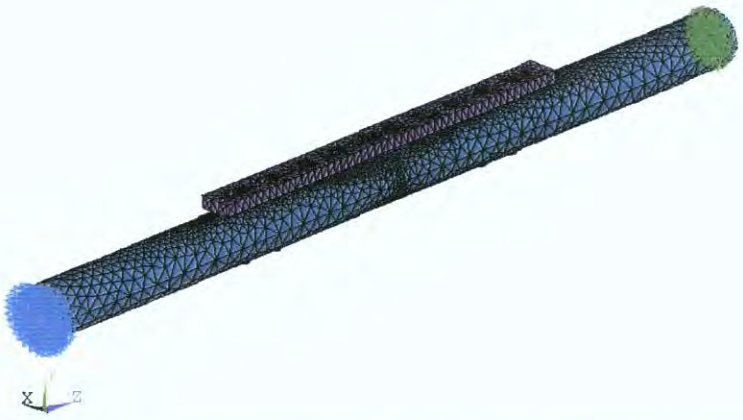

Fig 3.4. Axial loading to the proximal end. The Load applied to the nodes on the proximal end is coloured red.

3.3. Displacement Analysis of load-bearing fixation

The FE model from above was used to analyse and quantify the magnitude of displacement at the fracture site by altering the following parameters:

1. Load applied to bone.
2. Fracture gap.
3. Fracture translation in the X axis post fixation (i.e. moving the proximal bone segment laterally from 9mm to -9mm as shown in the figure below (Fig. 3.5).

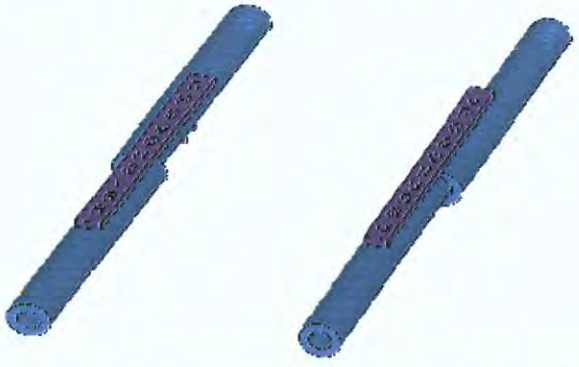

Figure 3.5 Range of fracture translations used in the FE analysis from -9 to 9mm in the X-axis post plate fixation.

4. Fracture angle post fixation, this ranged from 6° to -6° as shown below (Fig 3.6).

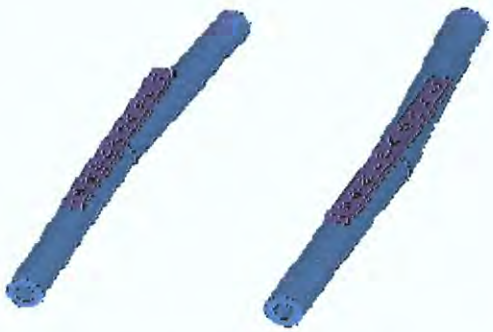

Figure 3.6 Range of fracture angles used in the FE analysis from 6 ° to -6 ° angle at the fracture site post plate fixation.

5. Combinations of different fracture translations and angle.
6. Number of screws.
7. Plate-bone distance.

Displacement results were then logged and analysed using Microsoft Excel spreadsheet.

3.4. Stress Analysis of load-bearing fixation

The same bone and fracture geometries were utilised from the previous analyses. This FE model was used to analyse and quantify the magnitude of stresses experienced by the implant when the innermost sets of screws are removed one at a time. This study would also determine the location of stresses experienced by the implant. The results were logged and analysed using Microsoft Excel spreadsheet.

3.5. Patient specific modelling – (case studies 1-3).

The FE strategies in the previous section were demonstrated using simple models, such as a tube to represent bone. However, patient specific finite element analysis requires exact knowledge of the material properties as well as the geometry of the bone and implant under investigation. This would avoid inaccuracies with regards to loading, fracture geometry and implant-bone geometric relationship.

For this part of the study three cases were selected, from a series of clinical cases where locking plate fixation was used in fractures of long bones, for finite element analysis. The three FE models were generated manually. Patient specific geometric information was obtained from AP and lateral plain radiographs.

A load equivalent to the weight of the patient was applied to each FE model. This axial load was simulated by fixing the distal end of the model and applying a force through the bone at the proximal end.

These three FE models were used to analyse and quantify the magnitude of displacement at the fracture site and the stresses experienced by the implant. The location of stresses experienced by the implant was also determined. The results were logged and analysed using Microsoft Excel spreadsheet.

3.6. Statistical analysis

Descriptive statistics were used to describe the basic features of the data in this study. Simple graphics analysis formed the basis of the data analysis.

Chapter 4 - Results

4.1. Displacement Analysis of load-bearing fixation

Displacement is a vector quantity which refers to "how far out of place an object is"; it is the object's overall change in position.

The FE model from the previous chapter was used to analyse and quantify the magnitude of displacement at the fracture site by altering the following parameters:

1. Load
2. Fracture gap
3. Fracture translation in the X axis post fixation
4. Fracture angle post fixation.
5. Combinations of different fracture translations and angles.
6. Number of screws.
7. Plate-bone distance.

4.1.1. Load

Five different loads ranging between 200 N and 1000 N were applied to the axial model. The results (displacement in the X, Y and Z axes and displacement sum) are plotted (fig. 4.1).

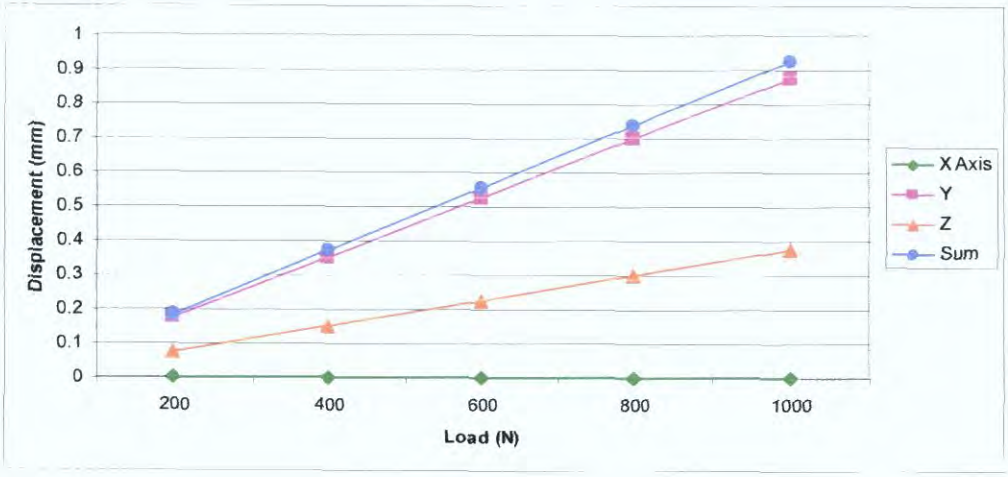

Fig 4.1. Load versus displacement graph

This graph demonstrates a linear relationship between the load applied to the bone in our FE model and the resulting displacement at the fracture site.

Axial stiffness of the implant construct was calculated (Fig. 4.2) using the nodal displacements at the fracture sites and the displacement sums above.

Stiffness= force / (displacement) N/m

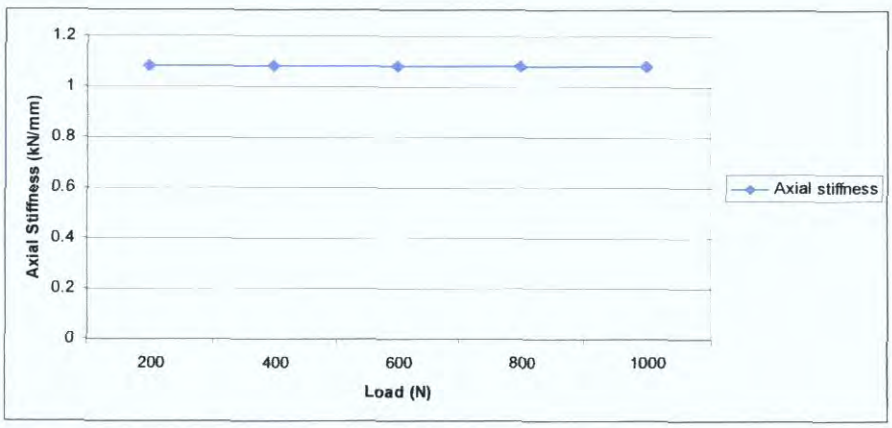

Fig 4.2. Axial stiffness of the implant construct at increasing loads. The graph demonstrates that increasing load did no affect the stiffness of the construct.

4.1.2. Fracture gap

A load of 400 N was applied to the FE model with fracture gaps ranging from 1mm to 5mm and the resulting displacement is shown below (Fig. 4.3).

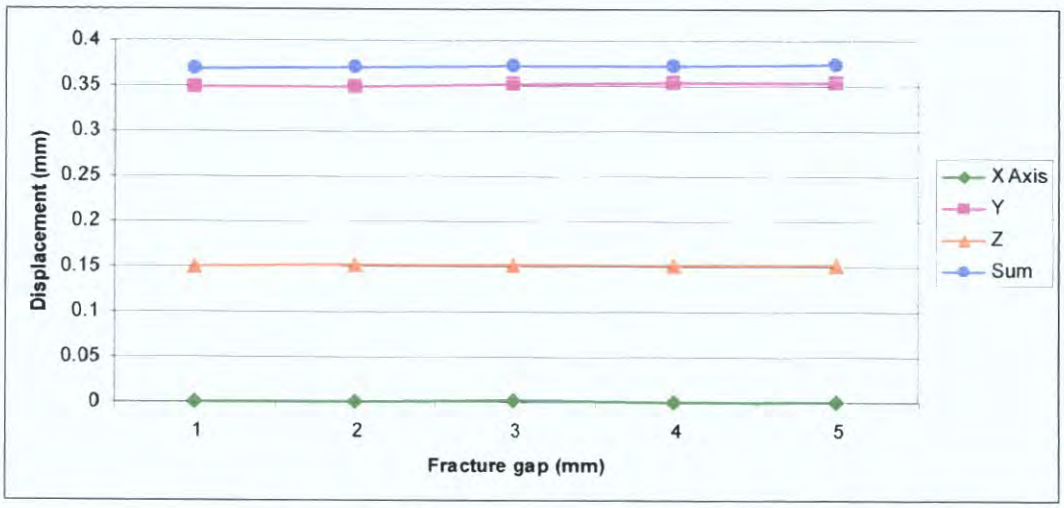

Figure 4.3. Displacement at the fracture site in FE models with different fracture gaps.

This graph demonstrates that increasing the fracture gap has almost no effect on the resulting displacement at the fracture site.

4.1.3. Fracture translation in the X axis post fixation

Here a load of 400 N was applied to the FE model with a fracture gap of 1mm at various fracture translations in the X axis. The results are shown in Fig. 4.4.

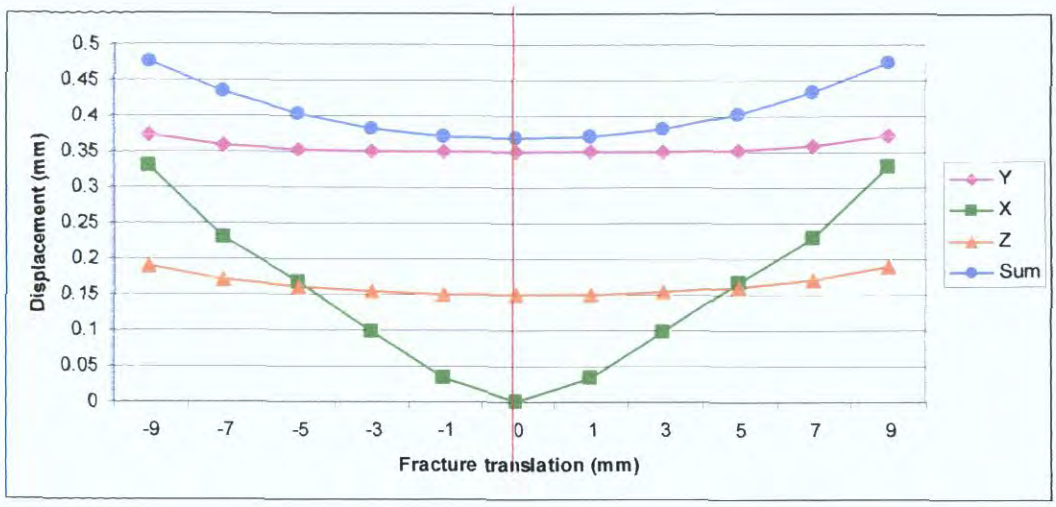

Figure 4.4. Displacement at the fracture site in FE models with various fracture translations in the X-axis.

This graph shows that increasing the translation results in increase in displacement at the fracture site, especially in the X-axis. The red line in the graph represents the axis of symmetry.

Using the (Sum of displacement) results from above the axial stiffness of the implant construct was calculated (Fig. 4.5)

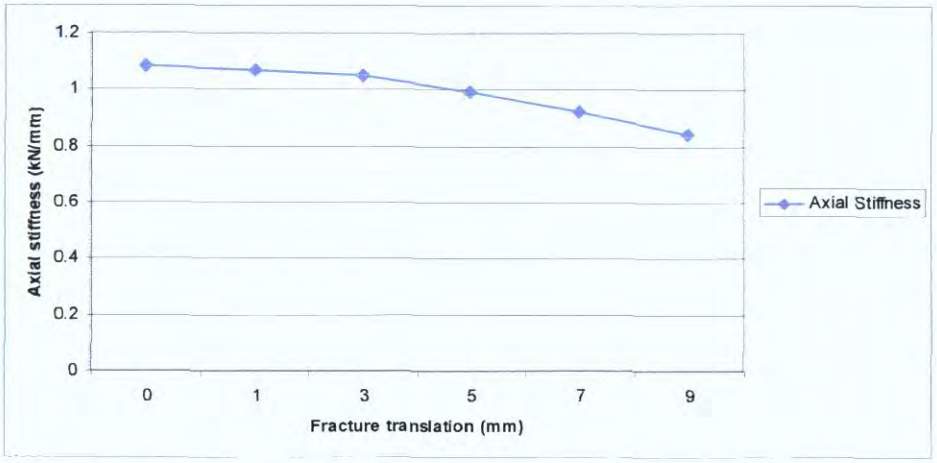

Figure 4.5. Axial stiffness of the implant construct at increasing fracture translations. The graph demonstrates that increasing the fixation translation results in a decrease in construct stability.

4.1.4. Fracture angle post fixation

In this part of the study a load of 400 N was applied to the FE model with a fracture gap of 1mm with zero translation at increasing angulation degrees at the fracture site. The results are shown in the graph below (Fig. 4.6).

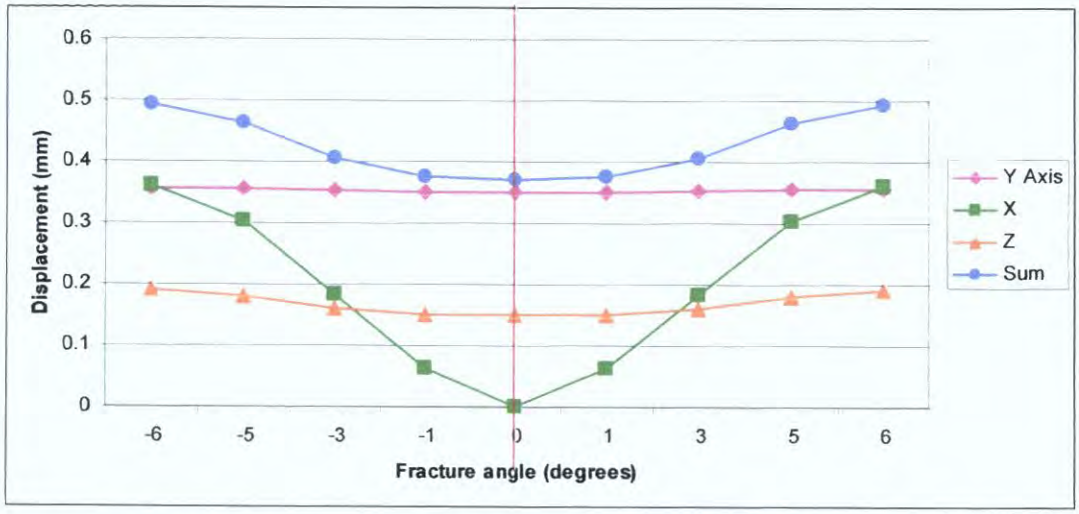

Figure 4.6. Displacement at the fracture site in FE models with different angulation degrees at the fracture site.

Increasing angulation results in an increase in displacement at the fracture site, more so in the X axis compared to the Y and Z axes. The red line in the graph represents the axis of symmetry.

Using the (Sum of displacement) results from above the axial stiffness of the implant construct was calculated (Fig. 4.7)

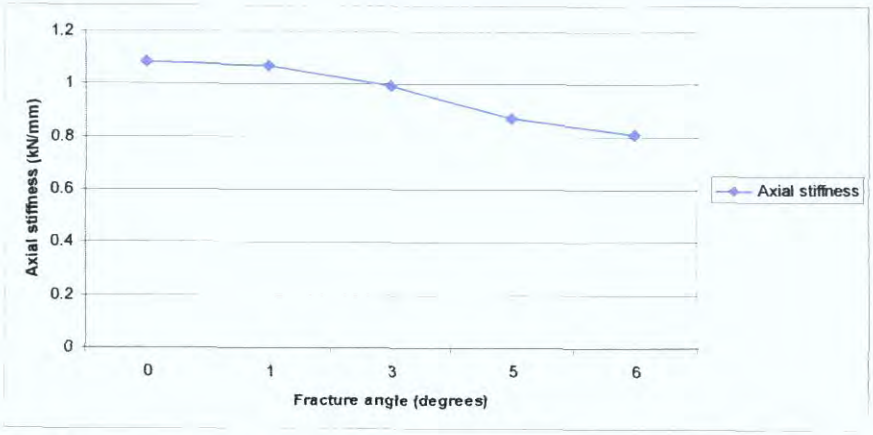

Figure 4.7 Axial stiffness of the implant construct at increasing fixation angles. The graph demonstrates that increasing fixation angle results in a decrease in construct stability.

4.1.5. Combinations of different fracture translations and angles

In this part of the study a load of 400 N was applied to the FE model with a fracture gap of 1mm. All possible combinations of fracture translations (-9 to 9mm) and angles (0 to 5 degrees) were analysed and the results plotted below (Fig. 4.8).

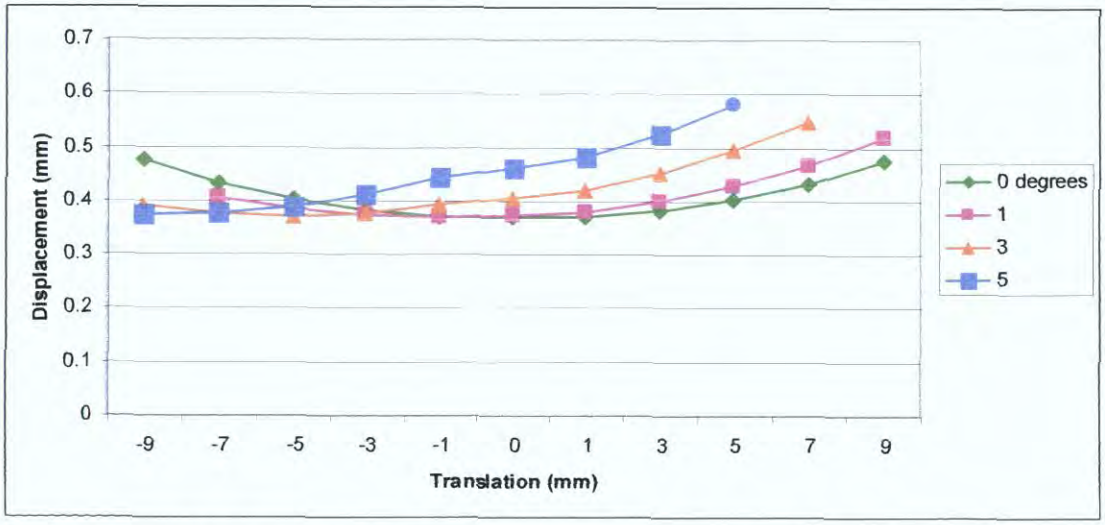

Figure 4.8. Displacement sum at the fracture site for the various combinations of different fracture translations and angles.

From the graph above it is noted that:

- For a zero degree fracture angle the displacement is minimal (0.369mm) when the translation is zero (this represents a perfectly reduced fracture).

- For a one degree fracture angle the displacement is minimal (0.370mm) when the translation is -1mm.

- For a three degree fracture angle the displacement is minimal (0.370mm) when the translation is -5mm.

- For a five degree fracture angle the displacement is minimal (0.372mm) when the translation is -9mm.

From this we can conclude that the minimal displacement in any of the displacement curves above remains almost unchanged, but the fracture translation at which the displacement is minimal varies with different fracture angles.

4.1.6. Number of screws

The displacement in FE models were compared for the cases when all ten locking screws were inserted, followed by removal of the two innermost screws, until 4 screws were remained (two on each side of the plate furthest from the fracture)(Fig. 4.9).

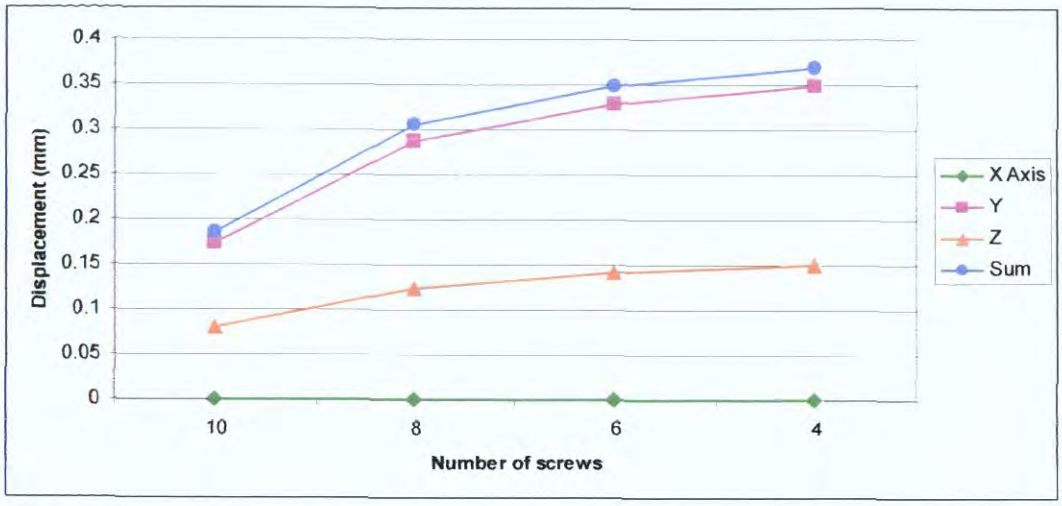

Figure 4.9 Displacement at the fracture site with different number of screws.

From the results the axial stiffness (Fig. 4.10) of the implant construct was calculated using the nodal displacements at the fracture sites.

Stiffness= force / (displacement) N/m

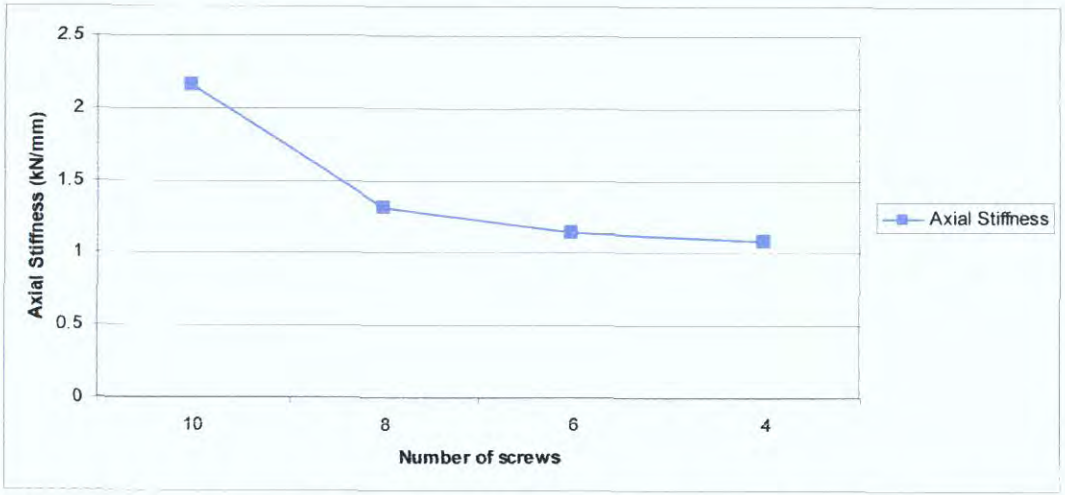

Figure 4.10. Axial stiffness of the implant construct with different number of screws.

On omission of the two innermost screws near the fracture site, axial stiffness decreased significantly by 39%. Removal of every further pair of innermost screws decreased the stability by about 9%.

4.1.7. Increasing plate-bone distance

Here the plate was raised from the bone 1mm at a time (range 0 to 6mm) and the displacement in the FE models was measured. (N.B. for every 1mm increase in bone-plate distance the lengths of the screws were increased by 1mm)(Fig 4.11)

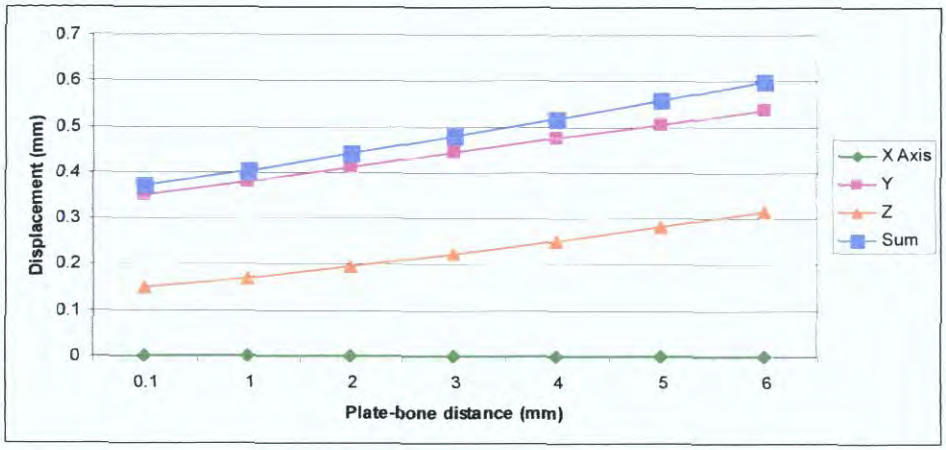

Figure 4.11. Displacement at the fracture site in the FE models at increasing plate-bone distances.

Using the (Sum of displacement) results the axial stiffness of the implant construct was calculated and plotted in (Fig 4.12). Increasing the distance from the plate to bone resulted in a decreased axial stiffness.

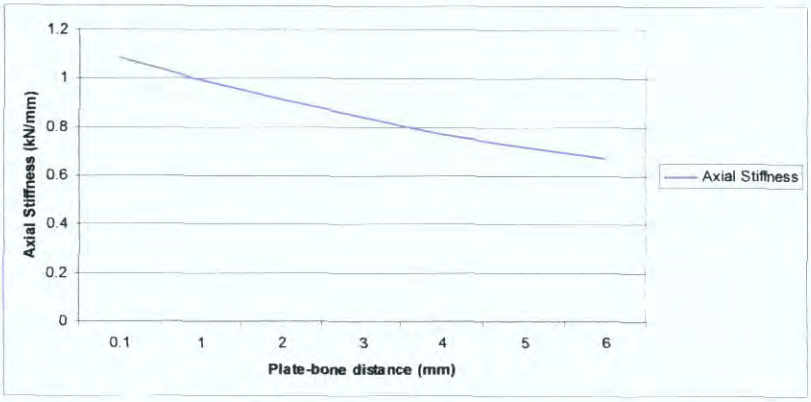

Figure 4.12 Axial stiffness of the implant construct at increasing plate-bone distances.

4.2. Stress Analysis of load-bearing fixation

The same bone and fracture geometries (i.e. same FE model) from the previous chapter was used to analyse and quantify the magnitude and determine the location of stresses experienced by the implant when the innermost sets of screws are removed one at the time.

4.2.1. All screws inserted

When all screws were inserted, the maximum stress in the implant was found at the screw-head junction. This stress concentration (751MPa) was above yield strength of stainless steel (σ_y = 235MPa) (Fig. 4.13), also, when the stresses in the plate were isolated, the maximum von Mises stress (294MPa) was still above yield strength of stainless steel. (Fig. 4.14).

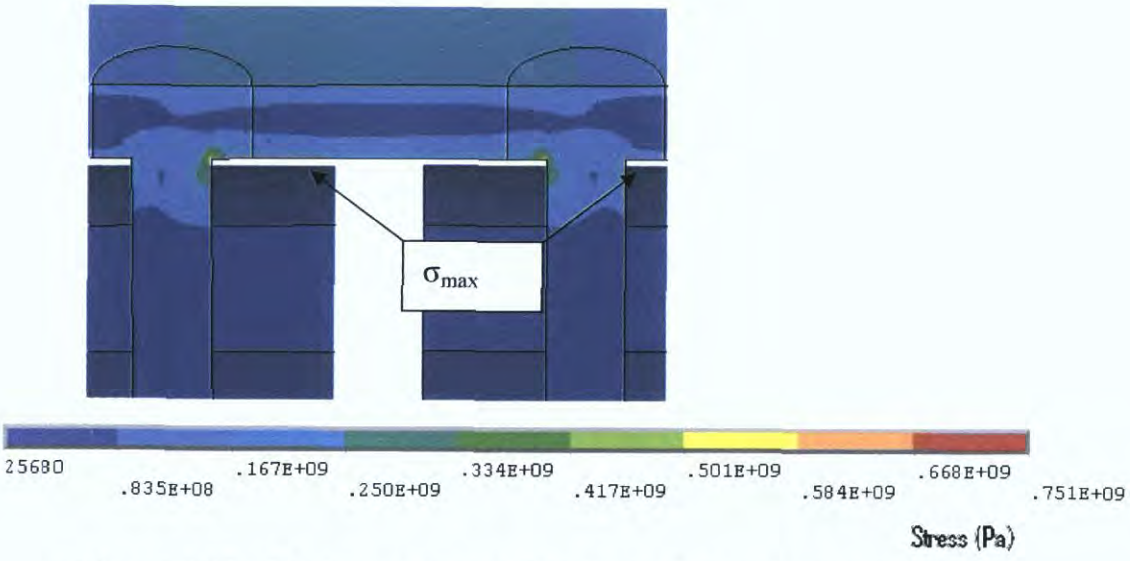

Figure 4.13. Maximum stress at junction of screw head and shaft.

The minimum plate stresses were found in the centre of the plate, where theoretically no stress exists (neutral axis). The maximum stresses were

found at the top and bottom of the plate, where it experiences tension and compression, respectively. This agrees with simple beam theory where the minimum stress is in the centre of the plate and the maximum stresses are furthest from the neutral axis (Fig. 4.15).

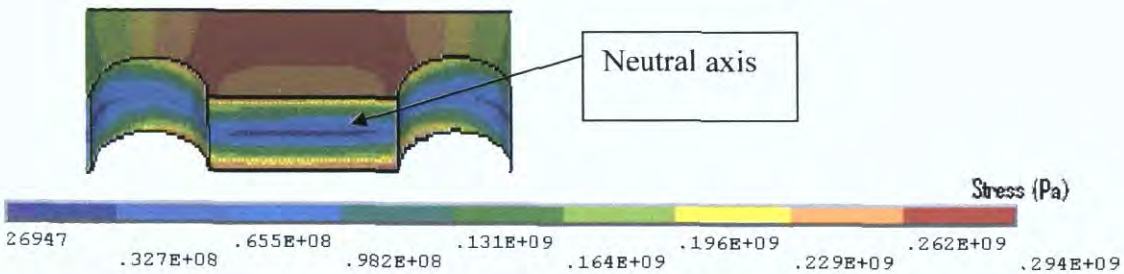

Figure 4.14. Stresses in experienced by the plate with all screws inserted.

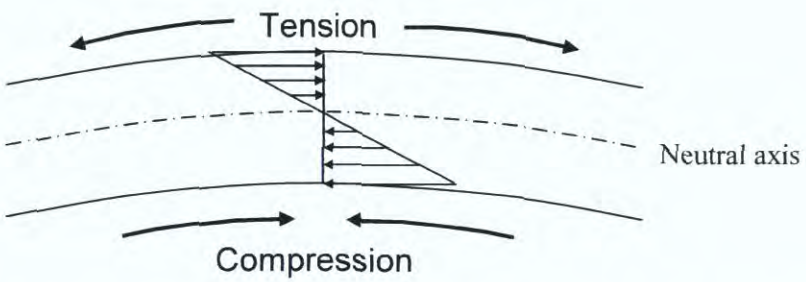

Figure 4.15. Element of plate under bending, with compression and tension side. The arrows represent the magnitude of stress at a given section of plate.

4.2.2 Two innermost screws removed

When the two innermost screws were removed, the plate stress decreased by 40% (176MPa) which is considerably lower than the yield strength of stainless steel. The maximum plate stresses were concentrated at the outer edges of the two middle screw holes at the portion of the holes that

accommodates the dynamic compression screws (Fig. 4.16). The maximum stresses were again found in the innermost screws (467 MPa), this represents a reduction of 38% compared to the previous case.

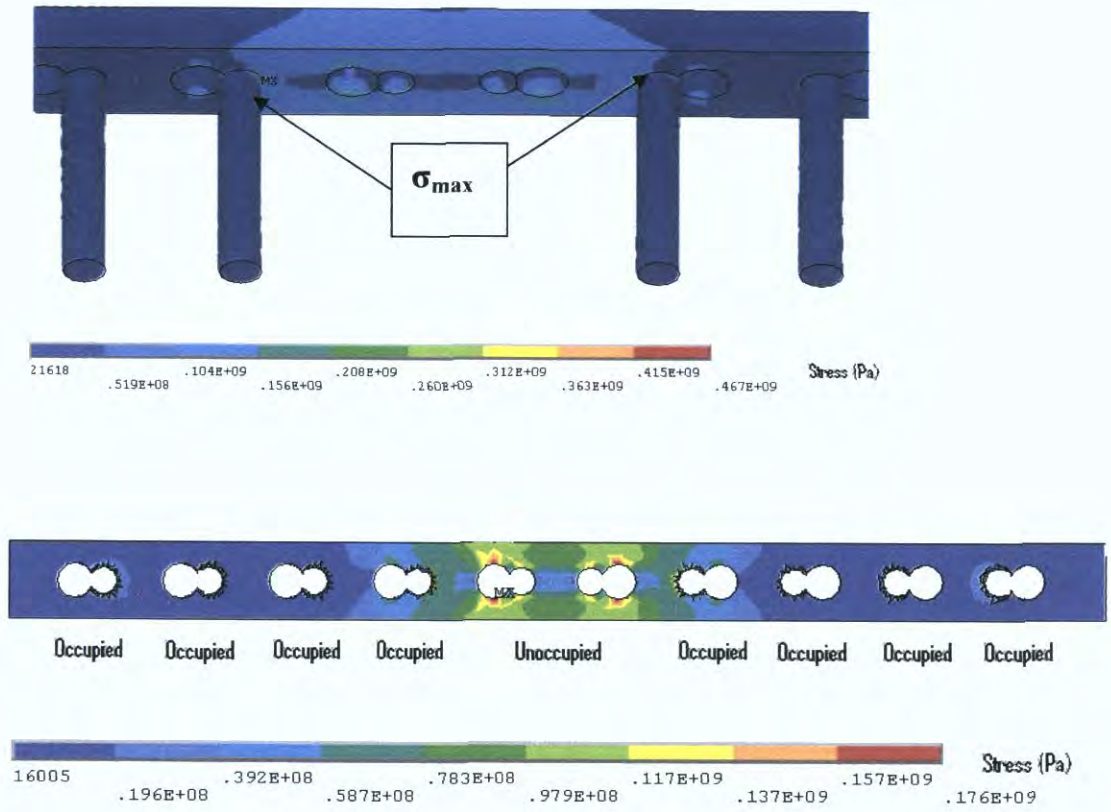

Figure 4.16. (top) Maximum stress at junction of screw head and shaft with two inner most screws removed, and (bottom) plate stress.

4.2.3 Four-six innermost screws removed

The maximum stresses where again found in the innermost screws (324MPa with the middle four screws removed) and (298MPa with the middle six screws removed) (Figs. 4.17-4.18). The screw stresses changed significantly from when all the screws were fully inserted to when the middle six screws were removed (751-298MPa). The maximum stresses in the screws were above yield strength of stainless steel.

The maximum plate stresses remained concentrated at the outer edges of the two outermost empty screw holes at the portion of the holes that accommodate the dynamic compression screw, (130MPa with the middle four screws removed and 109 with the middle 6 screws removed)

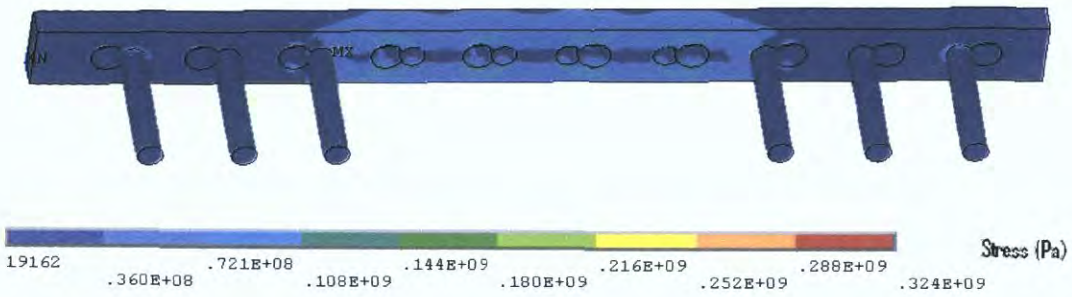

Figure 4.17. Implant stress contour when four of the inner most screws were removed. Note: the maximum plate stress was 130MPa

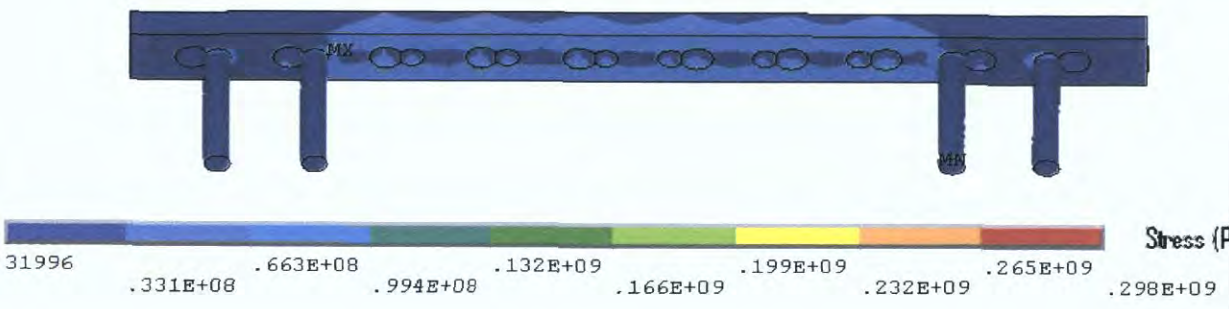

Figure 4.18. Implant stress contour when six of the inner most screws were removed. Note: the maximum plate stress was 109MPa.

4.2.4 Summary

The graph below (Fig 4.19) shows the summary of stress analysis results obtained above.

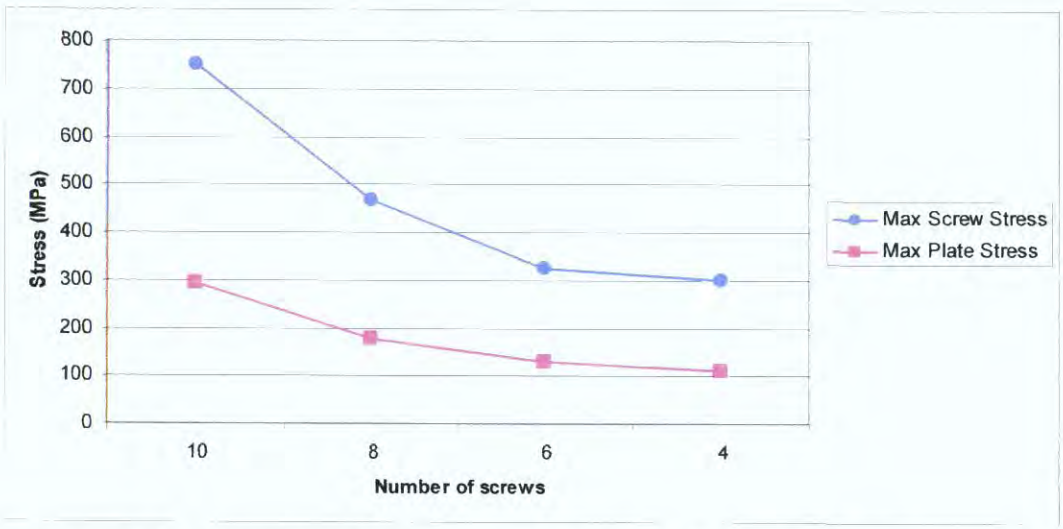

Figure 4.19. Maximum stresses in the screws and plate as the innermost sets of screws were removed one at a time

The stress concentrations were localized to a point or a specific region of the implant. The majority of stresses were therefore below the yield stress, and hence the implant would not have deformed permanently. Despite this, these stress concentrations can indicate where fatigue failure might occur.

Chapter 5 - Patient specific FE modelling

Case Study 1[1]

A 23-year-old man with no background history sustained a transverse fracture (Fig. 5.1a) of the right tibia and fibula (AO 42 A3) after receiving a kick on the shin while playing Gaelic football. The fracture was stabilised with a 4.5mm Narrow LCP (Fig. 5.1b&c) with 10-Combi holes using 6 looked screws (two screws at either end of the plate and two screws adjacent to the two middle holes over the fracture site).

Six months later on follow-up radiography there was no visible callus formation at the fracture site. At this stage he underwent removal of the two inner-most screws. Radiography six months after the 2nd procedure revealed that the fracture had healed with marked callus formation (Fig. 5.1d).

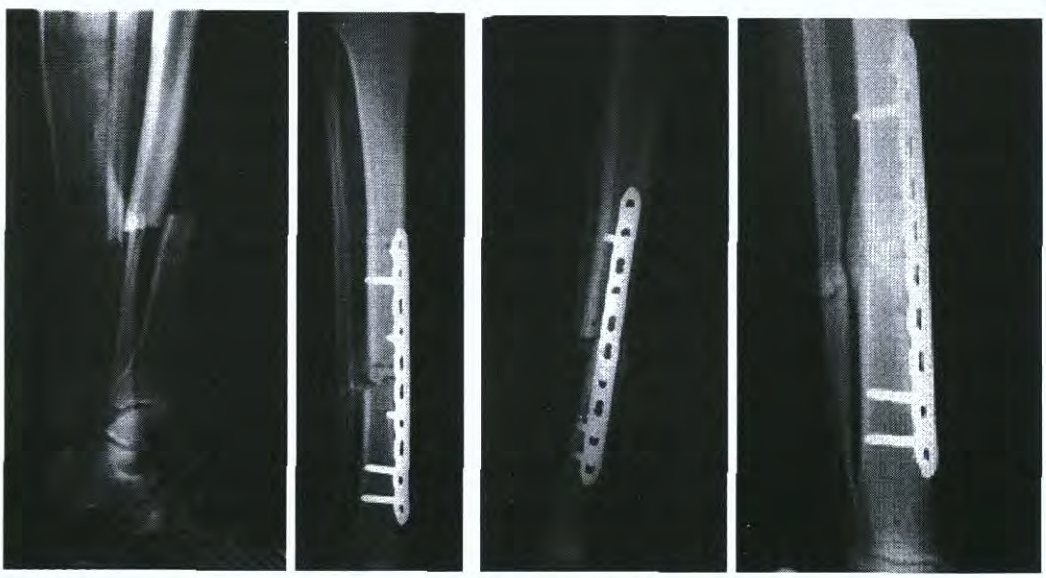

a. b. c. d.

Figure 5.1. Clinical case of a tibial fracture stabilised with a 4.5mm LCP in a 23 years old patient. The preoperative (a), post operative (b&c) and follow-up radiographs six months post removal of the two inner-most screws (d) are shown.

[1] This FE model was built for a related collaborative research programme by Damien Comiskey (PhD Student) and Dr Bryan McDonald (Senior Lecturer, DCU).

Finite Element Analysis

Two finite element models were created by using patient specific geometric information obtained from plain radiographs (fig. 5.2). Model (A) represents the fracture fixed with a 4.5mm narrow LCP using 6 locked screws. In model (B) the two innermost screws have been removed. The number and position of screws used in each scenario is shown in (fig. 5.3). A Load of 833 N (patient weight 85kg) was then applied through the bone at the proximal end in each case.

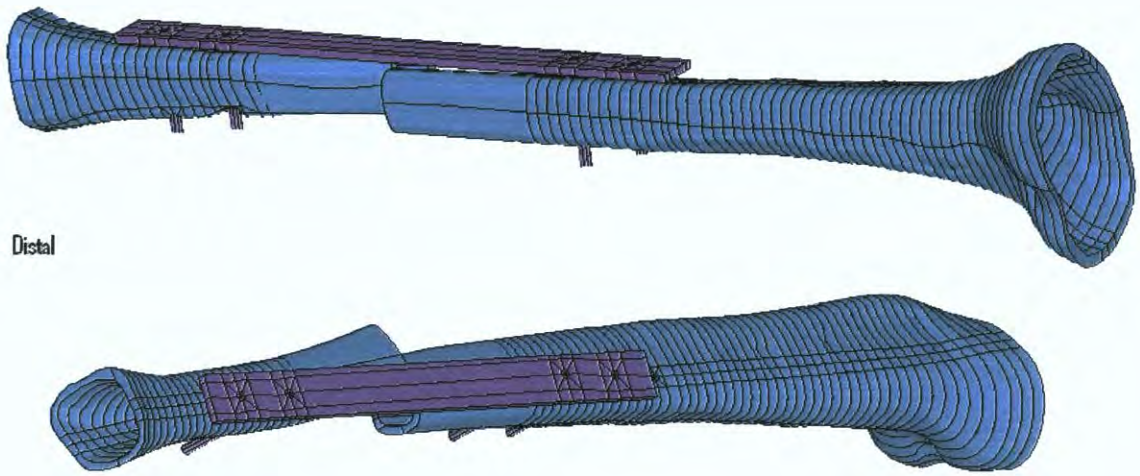

Figure 5.2. Finite element model of the locking plate system (Case study 1)

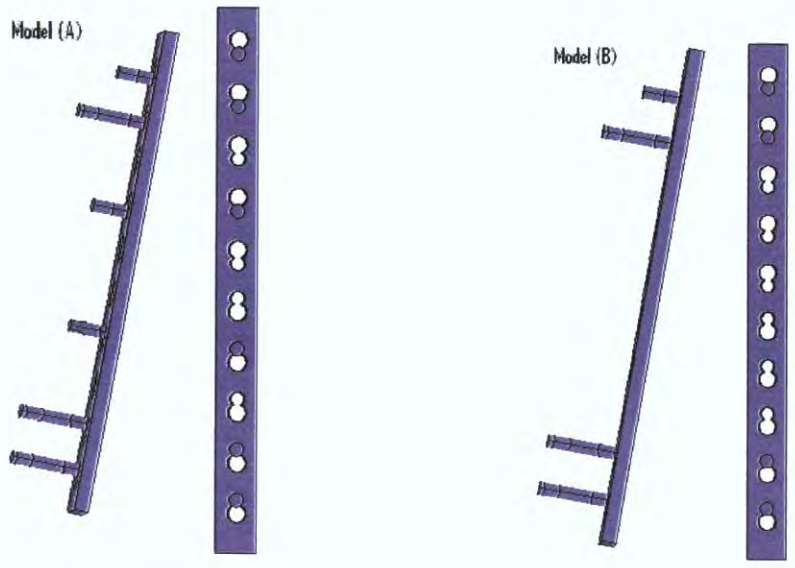

Figure 5.3 Position and number of screws in models (A) and (B).

Results

The working length had an important effect on construct stability. By omitting the two innermost screws near the fracture site, the construct became more flexible (axial stiffness decreased by 18%) (Fig. 5.4).

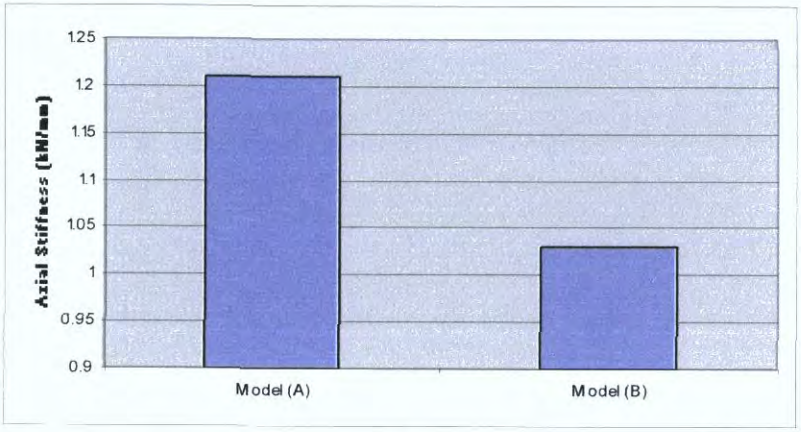

Figure 5.4 Axial stiffness of the implant construct before (Model A) and after (Model B) removing the two innermost screws.

It appears to be essential that a sufficient length of plate is left without screws at the level of the fracture to achieve adequate flexibility of the construct and to promote callus formation through micro-motion. After removal of the two screws, gap closure occurred under load conditions (Fig. 5.5).

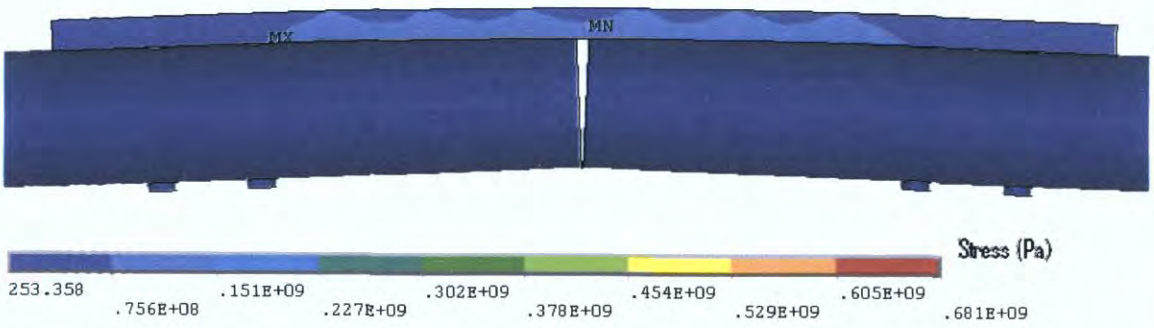

Figure 5.5 Implant stress contour (Model B). Note: the maximum plate stress was 235MPa.

Also, the maximum von Mises stress in the plate and the two innermost screws decreased significantly when the bridging length was increased (model B) because bone contact occurred under load conditions. Removing the two innermost screws, reduced the stress in the plate by 58% and in the screw by 66% (Fig. 5.6).

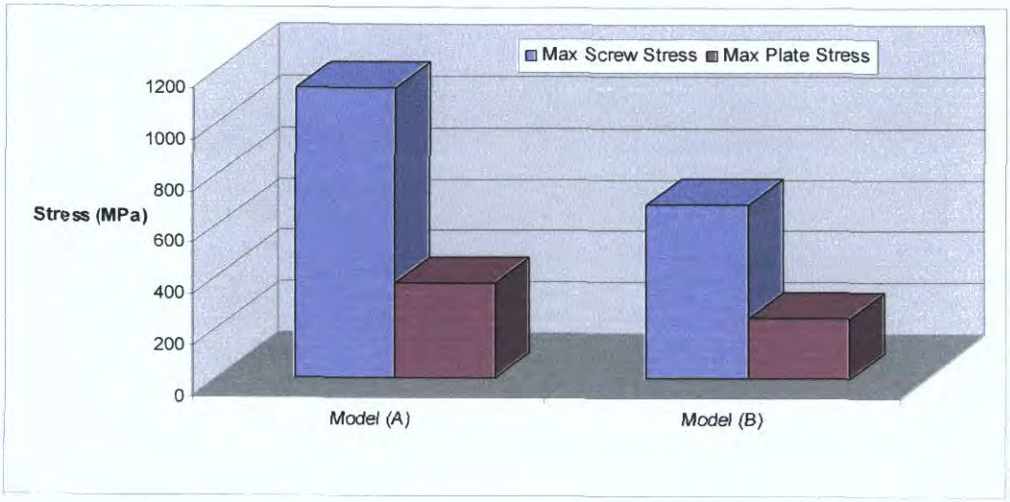

Figure 5.6 Max stress plate and screw stress before (Model A) and after (Model B) removing the two innermost screws.

The stress concentrations were localised to a point or a specific region of the implant. The majority of stresses were therefore below the yield stress, and hence the implant would not have deformed permanently (Fig. 5.7). Despite this, these stress concentrations can indicate where fatigue failure might occur.

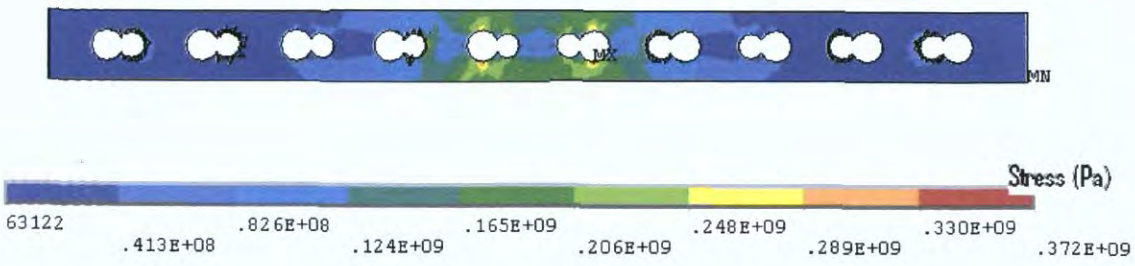

Figure 5.7 Plate stress (Model A), note the majority of stresses were below the yield stress (235MPa).

Case Study 2 [1]

A 74-year-old woman with osteoporosis, polymyalgia Rheumatica and COAD suffered a spiral fracture of the distal femoral diaphysis (AO 32 B1). The fracture (Fig. 5.8a&b) was treated by open reduction and stabilisation with a 15-hole LCP Distal Femur Plate (Fig. 5.8c&d) using 13 looked screws (one hole in the shaft portion of the plate at the fracture site and one hole in the head of the plate were left unoccupied).

Figure 5.8 Clinical case of a femoral fracture in a 74 year old patient treated with a LCP. The preoperative (a&b), post operative (c&d), implant failure at 22weeks (e&f) and follow up radiographs one year after IM nailing (g) are shown.

[1] This FE model was built with significant input from Dr Bryan McDonald (Senior Lecturer, DCU).

Follow-up radiographs after 22 weeks (Fig. 5.8e&f) revealed plate breakage at the middle part of the original fracture. No callus formation was visible at the level of the fracture. She then underwent IM nailing of her right femur and subsequent radiography after 1 year revealed complete consolidation with marked callus formation (Fig. 5.8g).

Finite Element Analysis

A finite element model (Fig. 5.9) was created by using patient specific geometric information obtained from plain radiographs. A load of 539N (patient weight 55kg) was then applied through the femoral head.

Results

Due do the very short working length (one unoccupied screw hole over the fracture site) and insertion of locking screws at the level of the fracture passing through the fracture line, the construct was rigid with an axial stiffness of (2.0 kN/mm). This hindered the micro-motion needed for callus formation.

The maximum Von Mises stress in the plate (299MPa) was found at the outer edges in the unoccupied screw-hole over the fracture site (Fig. 5.10). This is significantly higher than the yield strength of stainless steel (235MPa). Failure of the fracture to heal at 22 weeks meant that the stresses experienced by the implant remained under the load-bearing rather than the load-sharing scenario. Fatigue failure occurred at this site due to cyclic loading past the yield stress

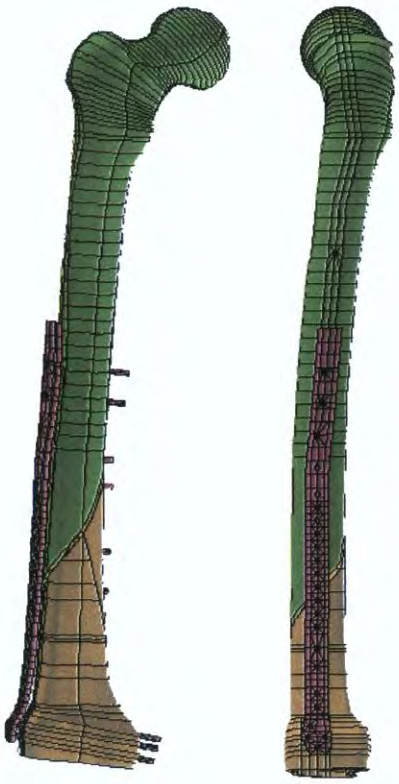

Figure 5.9 Finite element model of the locking plate system (Case study 2).

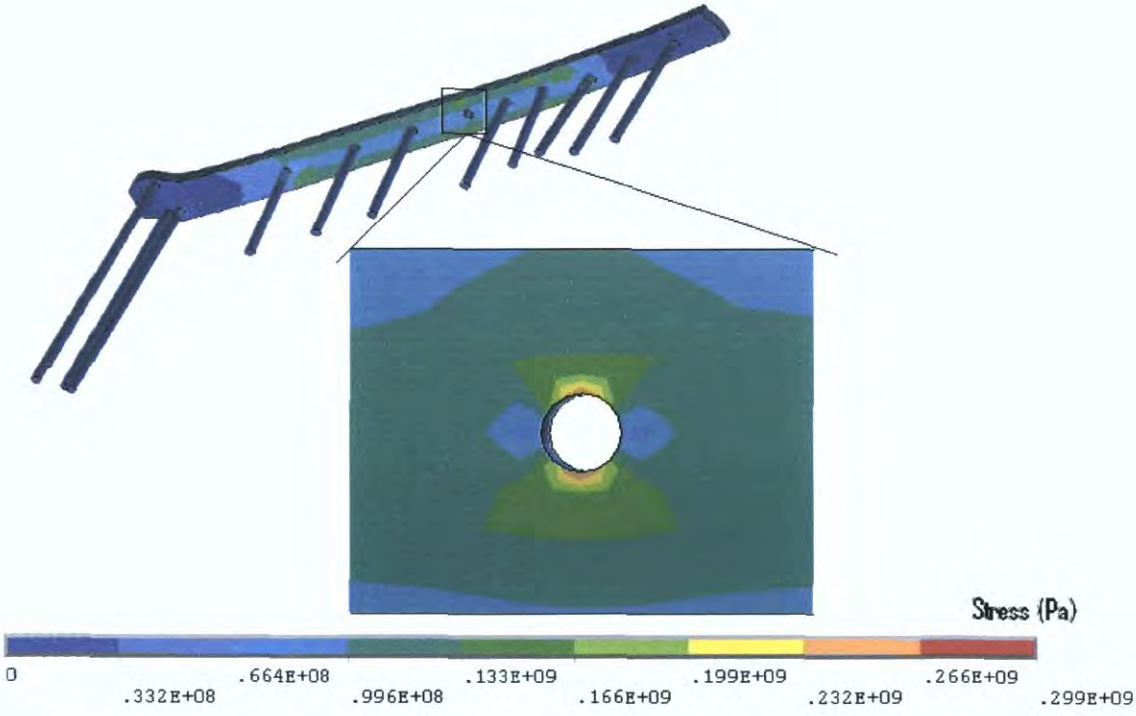

Figure 5.10 Stresses experienced by the LCP plate. Note: the maximum plate stresses were concentrated at the edges of the unoccupied screw-hole where fatigue failure occurred.

Case Study 3 [1]

A 91-year-old nun with background history of melanosis coli and osteoarthritis tripped and fell indoors sustaining a spiral fracture (Fig. 5.11a&b) of the right distal femoral diaphysis (AO 32 B1). The fracture was stabilised with a LCP Distal Femur Plate (Fig. 5.11c&d) using 7 locked screws and one partially threaded cancellous screw (6 screw holes were left unoccupied over the fracture site).

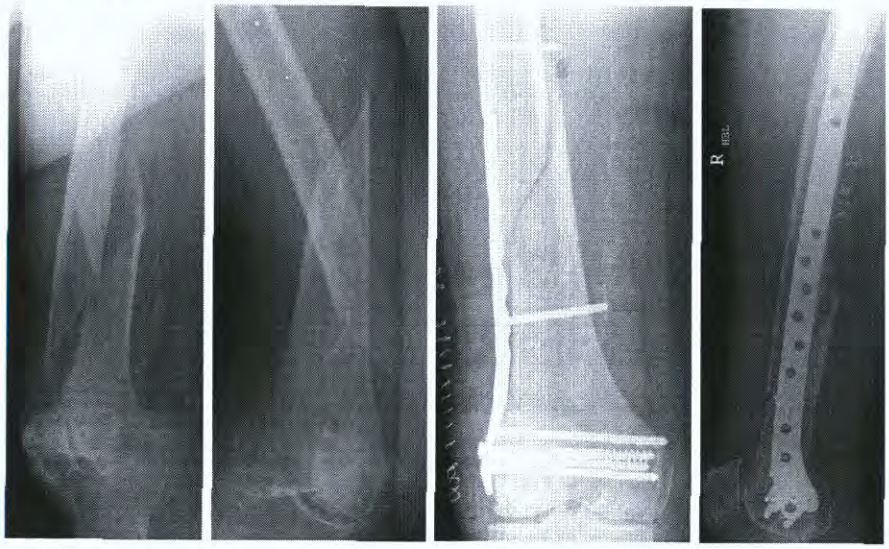

a. b. c. d.

e. f.

Figure 5.11 Clinical case of a femoral fracture in a 91 years old patient treated with a LCP. The pre-operative (a&b), post operative (c&d), and follow-up radiographs at 6 months post-op (e&f) are shown.

[1] This FE model was built for a related collaborative research programme by Damien Comiskey (PhD Student) and Dr Bryan McDonald (Senior Lecturer, DCU).

Follow-up radiographs (Fig. 5.11e&f) 6 months later revealed indirect bone healing with marked callus formation

Finite Element Analysis

A finite element model was created by using patient specific geometric information obtained from plain radiographs. A load of 569N (patient weight 58kg) was then applied through the femoral head.

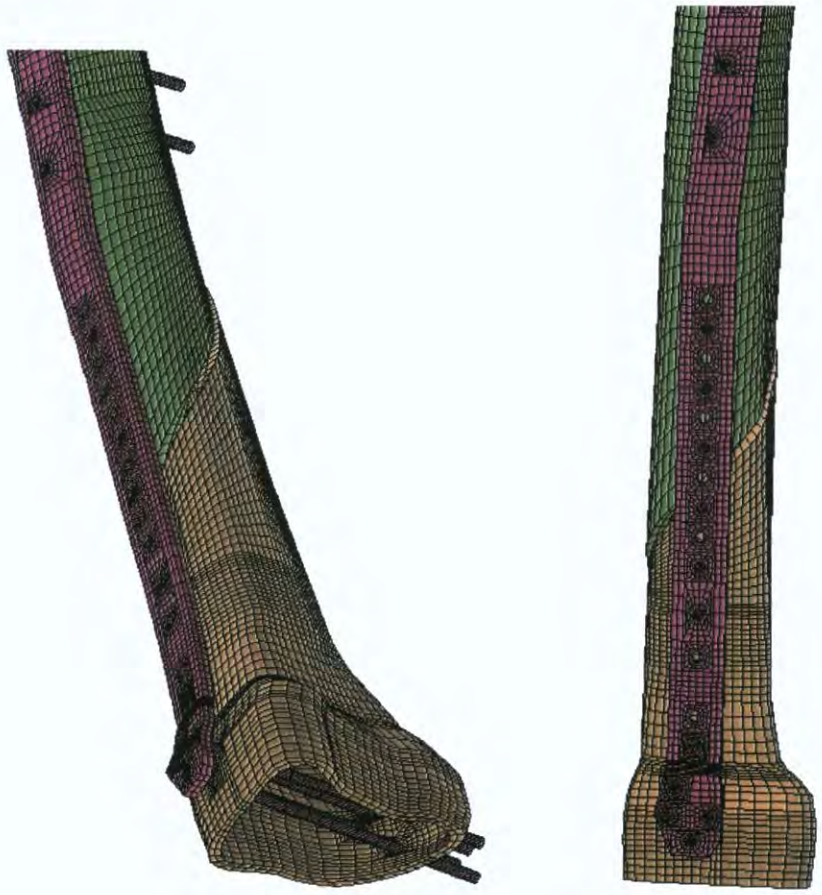

Figure 5.12 Finite element model of the locking plate system (case study 3).

Results

Due to the large working length (6 unoccupied screw holes over the fracture site) the construct was relatively flexible with an axial stiffness of (0.9 kN/mm). This seems to have promoted callus formation through micromotion.

The maximum von Mises stress (149 MPa) was found in the innermost screw distal to the fracture site. The maximum plate stresses (117 MPa) were concentrated at the outer edges in the unoccupied screws-holes over the fracture site. It should be noted that all stress concentrations in this case were below yield strength of stainless steel (235 MPa).

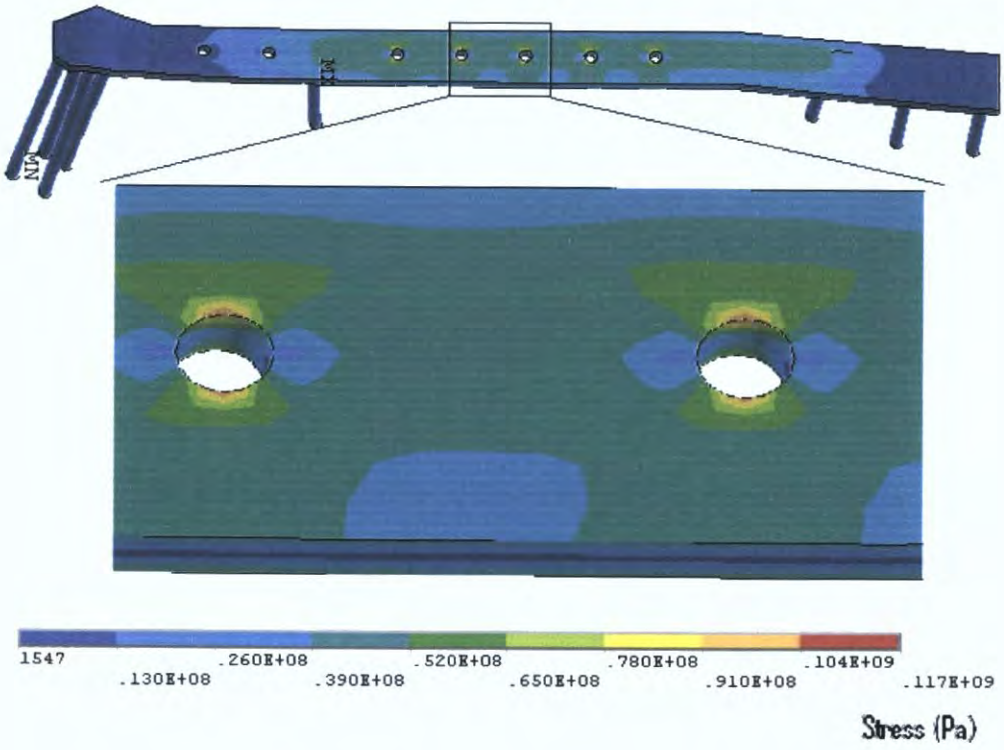

Figure 5.13 Stresses experienced by the LCP plate. Note: all stress concentrations in this case were below yield strength of stainless steel.

Chapter 6 - Discussion

The goal of this study was to apply the finite element method to aid the pre-operative planning process in fracture fixation. The focus of this study was not based entirely on the modelling of fractures fixed using locking plate techniques but rather how the finite element models will accurately predict complications such as implant failure or non-union and allow for a deeper understanding of the factors influencing these complications.

In the past, the appearance of callus in plate osteosynthesis was assumed to indicate a lack of stable fixation. Today, indirect healing with callus formation is no longer regarded as a disturbance to healing but a welcome sign of a positive bone reaction. However, in the stabilisation of fractures of long bones there is a fine line between flexible fixation, which enhances callus formation and improves the healing process, and an unstable fixation, which leads to non-union and/or implant failure.

When selecting an internal fixator for plate osteosynthesis, the main problem is to determine how the mechanical environment of the fracture and implant failure can be controlled. The first clinical results with internal fixators were promising [5, 35], although determining the number and position of screws was mainly based on clinical experience with conventional plates as described in numerous studies [4, 22]. The present study primarily focused on understanding the control mechanisms of stability and fatigue failure for internal fixators such as the LCP.

The working length had a significant effect on construct stability. By omitting the two innermost screws (one on either side of the fracture), the construct became more flexible by about 39% in compression. These results are in agreement with those of biomechanical investigations for conventional

plating techniques [17]. Removal of further pairs of innermost screws further increased flexibility but rather modestly.

It has been shown that axial stiffness is reduced when the same numbers of screws are used in a longer plate than in a shorter plate [55]. Therefore Stoffel et al. [55] suggests that long plates should be used to optimise axial stability and that the plastic deformation of the plate is reduced when the screws closest to the fracture site are removed. This results because when the working length of the plate is increased, more flexibility is tolerated.

Gautier and Sommer [30] note that the absolute minimal arrangement of screws is two monocortical screws placed in each main fragment of bone. If the two monocortical screws are replaced with bicortical screws the bone-screw interface improves, however, there is no improvement in fatigue life. Therefore, the recommendation is that there are a minimum of three screws in each main fragment [30, 55].

Increasing the distance between the plate and the bone significantly affected construct stability. By increasing this distance from 1mm to 5mm, axial stiffness decreased by 27% (7-9% for every 1mm) as the unsupported free part of the screw between the plate and bone increases, it produces a greater lever arm effect during compression testing and hence a weaker construct.

A recent study by Ahmad et al. [1] showed that LCPs at 2mm and flush to the bone responded in a similar manner and failed at significantly higher load than the plates at 5mm in static loading. The plates at 5mm also showed a much higher displacement in cyclic axial and torsion testing. Therefore it is recommended to place the plate at a distance less than or equal to 2mm.

The fracture gap had no effect on the construct stability when no bone contact (load sharing) occurred during loading. Stofell et al. [55] found the LCP plate to behave differently when bridging a small fracture gap, compared to a larger gap when no load sharing can occur during dynamic loading, such that when bridging a large gap the screws should be kept close to the centre of the plate because of the decreased Von Mises stresses and the increased cycles to failure.

Increasing the axial loading resulted in a proportional increase in displacement at the fracture site (linear relationship) when no bone contact occurred. The increase load did not affect the stiffness of the construct.

Increasing fracture angle reduced construct stability. By increasing the angle from 0 (perfect reduction) to 5 degrees in the lateral axis, construct stability decreased by 19%. Similarly increasing the fracture translation from 0 (perfect reduction) to 5mm in the lateral axis reduced construct stability by 8%.

Analysis of the combinations of different fracture translations and angles showed that the maximum achievable construct stability remained unchanged for the different fracture angles. However, the fracture translation at which the maximum stability is achievable varies with the different fracture angles.

In our finite element calculations under pure axial compression, axial stiffness values were found to be similar to those derived from the in vitro tests carried out by Ahmad et al. [1] and Stoffel et al. [55].

The stress analysis demonstrated that the maximum von Mises stresses were found in the innermost screws at the screw-head junction. When the stresses in the plate were isolated, the maximum von Mises stresses were

concentrated at the outer edges of the two outermost empty screw holes at the portion of the holes that accommodate the dynamic compression screw. Maximum stresses decreased with the removal of the two innermost screws, a pair at a time. The reduction in the stresses was most significant when the first pair of innermost screws were removed.

The first case study highlighted the importance of the working length on the construct stability. By increasing the working length from four to six empty screw-holes over the fracture site, the construct became 18% more flexible in compression. The resulting increase in interfragmentary motion promoted indirect healing with the formation of callus.

In this case, as the system become more flexible (longer bridging length) and bone contact occurred, the stress in the plate was reduced by 58% (fig 5.6) since less force was needed to achieve interfragmentary contact and this was reflected in lower peak stress magnitudes.

Hardware failure (plate failure, or screw breakage) is a complication that has been reported to occur in as many as 7% of plate fixations [49]. In the second case study, plate breakage occurred as a result of an inappropriate fixation technique, rather than the choice of plate. The fixation involved the use of locked screws at the level of the fracture passing the fracture line. The distribution of the screws, which have been shown to be important factor determining the stability of the fixation, was similar to those used in a conventional compression plate. [21, 55]. However, the insertion of locking screws at the level of the fracture reduces the flexibility of the implant [55] which hinders the micromotion needed for callus formation. Fatigue failure eventually occurred due to cyclic loading past the yield stress of the LCP. Failure occurred in the region of maximum von Mises stress in the plate at the outer edges of the unoccupied screw-hole over the fracture site.

In 2005, Gardner et al. [29] reported in vitro biomechanical results of the LCP when compared with the LC-DCP. While the LC-DCP continually failed at the most distal screw the LCP followed no specific pattern of failure. On the contrary Stoffel et al. reported in 2003 that in bridge plating with the LCP plate failure mostly occurred at the DCP hole near the fracture gap, which is in agreement with the finding of this study. One possible reason for such discrepancies is the specimen used. Gardner et al. [29] performed their test using cadaveric radii while stoffel et al. [55] used composite cylinders.

In the third case study the long working length of the construct made it relatively flexible. This allowed healing through lateral callus formation from the micro-motion induced by the weight-bearing.

The Von Mises stresses in the LCP plate and screws are considerably lower in the third case-study compared to the other two. This is due not only to the large working length but also the relatively longer plate [55]. As relatively few screws were inserted the plate leverage increased which decreases the individual load on each screw. Leaving six empty screw-holes over the fracture meant that larger area of stress distribution on the plate was achieved. Bending a plate over a longer segment reduces the local strain, resulting in a protective effect against fatigue failure of the implant.

Sommer et al [54] reported on four cases of implant failure as a result of technical error and not of the implant itself. Therefore it is evident that special training and care must be taken in planning such that implant application is optimised.

Chapter 7 - Conclusions

Patient specific modelling has become more prevalent as computer power and knowledge of the influences of mechanical stimulus on tissue differentiation has increased. The success of pre-operative patient specific modelling, however, relies on automatic and efficient modelling of the patient's anatomy, fast solution times and reliable results.

The results of this paper have shown that the finite element method can provide an excellent prediction of the behaviour of a fracture fixation device.

Based on the present results, the following conclusions can be made for the locking compression plate for fractures of the lower extremity:

- By increasing the working length the construct becomes more flexible.

- The fracture gap had no effect on the construct stability when no bone contact occurred during loading.

- The axial stiffness of the construct decreased by increasing the distance between the plate and the bone.

- Increasing the post-fixation fracture angle or the fracture translation reduced the stability of the construct.

-Maximum Von Mises stresses were found in the innermost screws at the screw-head junction.

- Maximum plate stresses were found at the outermost empty screw holes.

- When the fracture gap is small both screw and plate stresses decreased with increasing the working length.

- When fewer screws are inserted the plate leverage increases which decreases the individual load on each screw.

Recommendation

For the clinical use of the LCP as a locked internal fixator in fractures with an interfragmentary gap of 1mm, at least two to four plate holes near the fracture gap should be omitted to allow fracture motion and bone contact to occur. This will also achieve a larger area of stress distribution on the plate and reduce the likelihood of fatigue failure due to cyclic loading.

Future considerations

There are a number of limitations to this study as the results are based on finite element analysis. FE results cannot be directly extrapolated to the clinical setting as the vivo situation is far more complex.

In addition, the applied load used in this model may not represent the multifaceted manner of loading that occurs in humans.

One of the weaknesses of the FE model is the absence of any contribution that increasing callus formation makes to the functioning of bone-implant construct. To address this issue, the morphology of healing bone tissue has to be modelled using computational optimisation techniques. A related collaborative research programme at DCU is currently working on the development of such models.

A significantly larger series of clinical cases must be retrieved for analysis and other factors influencing the mechanical conditions at the fracture site e.g. (plate length, plate thickness and position of screws) should also be investigated.

A series of biomechanical in vitro experiments using cadaveric bone to investigate the extent to which a locking plate could provide satisfactory stability will help validate our results.

References

1. Ahmad M, Nanda R, Bajwa AS, Candal-Couto J, Green S, Hui AC. *Biomechanical testing of the locking compression plate: When* does the distance between bone and implant significantly reduce construct stability? Injury 2007; 38(3): 358-364.

2. Akkus O, Korkusuz F, Akin S, Akkas N. Relation between mechanical stiffness and vibration transmission of fracture callus: an experimental study on rabbit tibia. Proc Inst Mech Eng H. 1998; 212(5):327-36.

3. An YH, Draughn RA. Mechanical testing of the bone and bone–implant interface. Boca Raton, New York, 2000.

4. Aro HT, Kelly PJ, Lewallen DG, Chao EY. The effects of physiologic dynamic compression on bone healing under external fixation. Clin Orthop Relat Res. 1990 Jul;(256):260-73

5. Babst R, Hehli M, Regazzoni P. [LISS tractor. Combination of the "less invasive stabilization system" (LISS) with the AO distractor for distal femur and proximal tibial fractures]. Unfallchirurg. 2001 Jun;104(6):530-5.

6. Beaupré GS, Carter D, Orr TE, Csongradi J. The importance of friction interfaces in mathematical models of plated long-bones. Proceedings of the 33rd Orthopaedic Research Society Meeting, 1986, 476.

7. *Beaupré GS, Carter D, Orr* TE, Csongradi J. Stresses in plated long-bones: The role of screw tightness and interface slipping. J Orthop Res. 1988; 6(1):39-50

8. Borgeaud M, Cordey J, Leyvraz PE, Perren SM. Mechanical analysis of the bone to plate interface of the LC-DCP and of the PC-FIX on human femora. Injury 2000; 31 Suppl 3:C29-36.

9. Chao CK, Hsu CC, Wang JL, Lin J. Increasing bending strength of tibial locking screws: Mechanical tests and finite element analyses. Clin Biomech (Bristol, Avon). 2007 Jan; 22(1):59-66.

10. Christel P, Cerf G, Pilla A. Time evolution of the mechanical properties of the callus of fresh fractures. Annals of biomedical engineering 1981; 9, 383-391.

11. Chui C, Wang Z. et al. A component-oriented software toolkit for patient specific finite element model generation. Advances in Engineering Software 2009; **40**,184–192.

12. Claes L, Wilke HJ, Augat P, Rübenacker S, Margevicius KJ. Effect of dynamization of diaphyseal fractures under external fixation. Clin Biomech (Bristol, Avon). 1995 Jul; 10(5):227-234

13. Claes L, Augat P, Suger G, Wilke HJ. Influence of size and stability of the osteotomy gap on the success of fracture healing.
J Orthop Res. 1997 Jul; 15(4):577-84

14. Claes LE, Heigele CA. Magnitudes of local stress and strain along bony surfaces predict the course and type of fracture healing.
J Biomech. 1999 Mar;32(3):255-66.

15. Claes L, Eckert-Hübner K, Augat P. The fracture gap size influences the local vascularization and tissue differentiation in callus healing. Langenbecks Arch Surg. 2003 Oct; 388(5):316-22.

16. Cole PA, Zlowodzki M, Kregor PJ. Less Invasive Stabilization System (LISS) for fractures of the proximal tibia: indications, surgical technique and preliminary results of the UMC Clinical Trial. Injury. 2003; 34 Suppl 1:A16-29.

17. Compte P, Straumann F. Influence of unoccupied holes on the fatigue behavior of bone fixation plates. In: Perren SM, Schneider E, eds. Proceedings of the European Society of Biomechanics: Current Interdisciplinary Research. Amsterdam: Martinus Nijhoff; 1985:459-464

18. De Bastiani G, Aldegheri R, Brivio LR. The treatment of fractures with a dynamic axial fixator. J Bone Joint Surg Br. 1984 Aug; 66(4):538-45

19. Duffy P, Trask K, Hennigar A, Barron L, Leighton RK, Dunbar MJ. Asssessment of fracture micromotion in distal femur fracture fixation with RSA. Clin Orthop Relat Res. 2006 Jul; 448:105-13

20. Egol KA, Kubiak EN, Fulkerson E, Kummer FJ, Koval KJ. Biomechanics of locked plates and screws. J Orthop Trauma. 2004 Sep; 18(8):488-93

21. Ellis T, Bourgeault CA, Kyle RF. Screw position affects dynamic compression plate strain in an in vitro fracture model. J Orthop Trauma. 2001 Jun-Jul; 15(5):333-7

22. El-Maraghy AW, ElMaraghy MW, Nousiainen M, et al. Influence of the number of cortices on the stiffness of plate fixation of diaphyseal fractures. J Orthop Trauma. 2001 Mar-Apr; 15(3):186-91

23. El-Sayed, A., Said, H.G.Z., Abdel-Aal, A., Farouk, O., 2001. Locked plate fixation for femoral shaft fractures.
Int Orthop. 2001; 25(4):214-8

24. Ferguson SJ, Wyss UP, Pichora DP. Finite element analysis of a hybrid fracture fixation plate. Med Eng Phys. 1996 Apr;18 (3):241-50

25. Florin M, Arzdorf M, Linke B, Auer JA. Assessment of stiffness and strength of 4 different implants available for equine fracture treatment: A study on a 20° oblique long-bone fracture model using a bone substitute. Vet Surg. 2005 May-Jun; 34(3):231-8

26. Frigg R, Appenzeller A, Christensen R, Frenk A, Gilbert S, Schavan R. The development of the distal femur Less Invasive Stabilization System (LISS). Injury. 2001 Dec; 32 Suppl 3:SC24-31.

27. Galibarov PE, Lennon AB, Prendergast PJ. Patient-specific finite element models based on radiographs for pre-operative planning. Proceedings of the 2007 Summer Workshop of the European Society of Biomechanics, Trinity College, Dublin, August 26-28 2007, 201-202.

28. Galuppo LD, Stover SM, Aldridge A, Hewes C, Taylor KT. An in vitro biomechanical investigation of an MP35N intramedullary interlocking nail system for repair of third metacarpal fractures in adult horses. Vet Surg. 2002 May-Jun;31(3):211-25

29. Gardner MJ, Brophy RH, Campbell D, Mahajan A, Wright TM, Helfet DL, Lorich DG. The mechanical behaviour of locking compression plates compared with dynamic compression plates in a cadaver radius model. J Orthop Trauma 2005; 19(9), 597-603.

30. Gautier E, Sommer C. Guidelines for the clinical application of the LCP. Injury 2003; 34, S-B63 – S-B76.

31. Goodship, A.E., Kenwright, J., 1985. The influence of induced micromovement upon the healing of experimental tibial fractures. J Bone Joint Surg Br. 1985 Aug;67(4):650-5

32. Hansmann, C. Eine neue Methode der fixierung der Fragmente bei complicierten Frakturen. Verh Dtsch Ges Chir 1886; 158.

33. Haerdi-Landerer C, Steiner A, Linke B, Wahl D, Schneider E, Hehli M, Frei R, Auer JA. Comparison of double dynamic compression plating versus two configurations of an internal veterinary fixation device: Results of in vitro mechanical testing using a bone substitute. Vet Surg. 2002 Nov-Dec; 31(6):582-8

34. Heiner AD, Brown TD. Structural properties of a new design of composite replicate femurs and tibias. J Biomech. 2001 Jun; 34(6):773-81

35. Karnezis IA, Miles AW, Cunningham JL, et al. "Biological" internal fixation of long bone fractures: a biomechanical study of a "noncontact" plate system. Injury. 1998 Nov; 29(9):689-95

36. Lauer SK, Aron DN, Evans MD. Finite element method evaluation: articulations and diagonals in an 8-pin type 1B external skeletal fixator. Vet Surg. 2000 Jan-Feb; 29(1):28-37

37. Lopez MJ, Wilson DG, Vanderby R, Markel MD. An in vitro biomechanical comparison of an interlocking nail system and dynamic compression plate fixation of ostectomized equine third metacarpal bones. Vet Surg. 1999 Sep-Oct; 28(5):333-40

38. Lopez MJ, Wilson DG, Trostel SS, Markel MD. An in vitro biomechanical comparison of two interlocking-nail systems for fixation of ostectomized equine third metacarpal bones. Vet Surg. 2001 May-Jun; 30(3):246-52.

39. Maldonado ZM, Seebeck J, Heller MOW, Brandt D, Hepp P, Lill H, Duda GN. Straining of the intact and fractured proximal humerus under physiological-like loading. J Biomech. 2003 Dec; 36(12):1865-73

40. McCartney W, Mac Donald BJ, Hashmi MSJ. Comparative performance of a flexible fixation implant to a rigid implant in static and repetitive incremental loading. Journal of materials processing technology 2005; 169:476-484.

41. Moorcroft CI, Ogrodnik PJ, Thomas PBM, Wade RH. Mechanical properties of callus in human tibial fractures: a preliminary investigation. Clin Biomech (Bristol, Avon). 2001 Nov; 16(9):776-82

42. Moorcroft C, Ogrodnik P, Thomas P. Reliability of fracture stiffness as a measurement of clinical union and visco-elastic properties of callus. Injury extra 2007; 38, 164.

43. Mora G, Forriol F. Mechanical analysis of the healing of different osteotomies fixed externally. Int Orthop. 2000; 24(5):295-8

44. Pauwels F. Eine neue theorie über den einflub mechanischer reize auf die differenzierung der stützgewebe. Z Anat Entwicklgesch 1960; 121, 478–515. Translated as A new theory concerning the influence of mechanical stimuli on the differentiation of the supporting tissues. In: Maquet P, Furlong R (Eds.), Biomechanics of the locomotor apparatus, Springer, Berlin, 1980, 375–407.

45. Perren SM. Physical and biological aspects of fracture healing with special reference to internal fixation. Clin Orthop Relat Res. 1979 Jan-Feb; (138):175-96

46. Radcliffe RM, Lopez MJ, Turner TA, Watkins JP, Radcliffe CH, Markel MD. An in vitro biomechanical comparison of interlocking nail constructs and double platting for fixation of diaphyseal femur fractures in immature horses. Vet Surg. 2001 Mar-Apr; 30(2):179-90

47. Radke H, Aron DN, Applewhite A, Zhang G. Biomechanical analysis of unilateral external skeletal fixators combined with IM-pin and without IM-pin using finite-element Method. Vet Surg. 2006 Jan; 35(1):15-23

48. Ramotowski W, Granowski R. Zespol. An Original method of stable osteosynthesis. Clin Orthop Relat Res. 1991 Nov; (272):67-75.

49. Riemer BL, Butterfield SL, Burke CJ, 3rd, et al. Immediate plate fixation of highly comminuted femoral diaphyseal fractures in blunt polytrauma patients. Orthopedics. 1992 Aug; 15(8):907-16

50. Sharma AK, Kumar A, Joshi GR, John JT. Retrospective study of implant failure in orthopaedic surgery. Medical journal of armed forces of India 2006; 62:70-72.

51. Shirazi-adl A, Ahmed AM, Shrivastava SC. Mechanical response of a lumbar motion segment in axial torque alone and combined with compression. Spine. 1986 Nov; 11(9):914-27

52. Simon BR, Woo S LY, Stanley GM, Olmstead SR, McCarty MP, Jemmott GF, Akeson WH. Evaluation of one-, two-, and three-dimensional finite element and experimental models of internal fixation plates. J Biomech. 1977; 10(2):79-86

53. Simon JA, Dennis MG, Kummer FJ, Koval KJ. Schuhli augmentation of plate and screw fixation for humeral shaft fractures: a laboratory study. J Orthop Trauma. 1999 Mar-Apr; 13(3):196-9

54. Sommer C, Babst R, Muller M, Hanson B. Locking comprssion plate loosening and plate breakage: a report of four cases. J Orthop Trauma 2004; 18(8), 571-577.

55. Stoffel K, Dieter U, Stachowiak G, Gächter A, Kuster MS. Biomechanical testing of the LCP – how can stability in locked internal fixators be controlled? Injury. 2003 Nov; 34 Suppl 2:B11-9

56. Taylor WR, Warner MD, Clift SE. Finite element prediction of endosteal and periosteal bone remodeling in the turkey ulna: effect of remodeling signal and dead-zone definition. Proc Inst Mech Eng 2003;217(5):349–56

57. Trease C, McIff T, Toby EB. Locking verus nonlocking T-plates for dorsal and volar fixation of dorsally comminuted distal radius fractures: A biomechanical study. J Hand Surg 2005; 30:756-763.

58. Veerabagu S, Fujihara K, Dasari GR, Ramakrishna S. Strain distribution analysis of braided composite bone plates. Composites science and technology 2003; 62:427-435.

59. Woo SLY, Akeson WH, Coutts RD, Rutherford L, Doty D, Jemmott GF, Amiel D, Jolla LA. A comparison of cortical bone atrophy secondary to fixation with plates with large differences in bending stiffness. J Bone Joint Surg Am. 1976 Mar; 58(2):190-5.

APPENDEX

4.1.1. Load

	200	400	600	800	1000 Load (N)
X	1.21E-08	2.41E-08	3.62E-08	4.82E-08	6.03E-08
Y	1.75E-04	3.49E-04	5.24E-04	6.99E-04	8.73E-04
Z	7.50E-05	1.50E-04	2.25E-04	3.00E-04	3.75E-04
Sum	1.85E-04	3.69E-04	5.54E-04	7.39E-04	9.23E-04

Displacement (m)

4.1.2 Fracture gap

	1	2	3	4	5 Fracture gap (mm)
X	2.41E-08	1.83E-07	1.38E-06	1.71E-08	7.63E-07
Y	3.49E-04	3.49E-04	3.52E-04	3.53E-04	3.54E-04
Z	1.50E-04	1.51E-04	1.51E-04	1.51E-04	1.51E-04
Sum	3.69E-04	3.70E-04	3.71E-04	3.72E-04	3.73E-04

Displacement (m)

4.1.3 Fracture Translation

	-9	-7	-5	-3	-1	0	1	3	5	7	9 Translation (mm)
Y	3.72E-04	3.58E-04	3.52E-04	3.50E-04	3.49E-04	3.49E-04	3.49E-04	3.50E-04	3.52E-04	3.58E-04	3.72E-04
X	3.29E-04	2.30E-04	1.66E-04	9.70E-05	3.38E-05	2.41E-08	3.38E-05	9.70E-05	1.66E-04	2.30E-04	3.29E-04
Z	1.89E-04	1.71E-04	1.60E-04	1.54E-04	1.51E-04	1.50E-04	1.51E-04	1.54E-04	1.60E-04	1.71E-04	1.89E-04
Sum	4.75E-04	4.33E-04	4.02E-04	3.81E-04	3.71E-04	3.69E-04	3.71E-04	3.81E-04	4.02E-04	4.33E-04	4.75E-04

Displacement (m)

4.1.4 Fracture Angle

	-6	-5	-3	-1	0	1	3	5	6	Angle
Y	3.55E-04	3.54E-04	3.52E-04	3.50E-04	3.49E-04	3.50E-04	3.52E-04	3.54E-04	3.55E-04	
X	3.61E-04	3.02E-04	1.82E-04	6.13E-05	2.41E-08	6.13E-05	1.82E-04	3.02E-04	3.61E-04	
Z	1.91E-04	1.79E-04	1.61E-04	1.51E-04	1.50E-04	1.51E-04	1.61E-04	1.79E-04	1.91E-04	
Sum	4.93E-04	4.62E-04	4.05E-04	3.74E-04	3.69E-04	3.74E-04	4.05E-04	4.62E-04	4.93E-04	

Displacement (m)

4.1.5. Displacement sum for combination of different fracture translations and angles

	-9	-7	-5	-3	-1	0	1	3	5	7	9	*Translation (mm)*
0	4.75E-04	4.33E-04	4.02E-04	3.81E-04	3.71E-04	3.69E-04	3.71E-04	3.81E-04	4.02E-04	4.33E-04	4.75E-04	
1		4.06E-04	3.84E-04	3.72E-04	3.70E-04	3.74E-04	3.79E-04	3.99E-04	4.28E-04	4.66E-04	5.20E-04	
3	3.90E-04	3.75E-04	3.70E-04	3.77E-04	3.93E-04	4.05E-04	4.19E-04	4.53E-04	4.95E-04	5.48E-04		
5	3.72E-04	3.75E-04	3.89E-04	4.12E-04	4.44E-04	4.62E-04	4.82E-04	5.26E-04	5.79E-04			

Angles

4.1.6 Number of screws

	10	8	6	4	No of screws
X	7.26E-07	6.51E-08	9.03E-08	2.41E-08	
Y	1.73E-04	2.86E-04	3.29E-04	3.49E-04	
Z	8.03E-05	1.24E-04	1.41E-04	1.50E-04	
Sum	1.85E-04	3.05E-04	3.49E-04	3.69E-04	

Displacement (m)

4.1.7 Bone-Plate Distance

	0.1	1	2	3	4	5	6	Bone-Plate distance (mm)
X	2.41E-08	1.25E-07	9.55E-08	8.56E-08	1.51E-07	1.18E-07	1.90E-07	
Y	3.49E-04	3.78E-04	4.10E-04	4.42E-04	4.74E-04	5.05E-04	5.37E-04	
Z	1.50E-04	1.70E-04	1.95E-04	2.21E-04	2.50E-04	2.82E-04	3.16E-04	
Sum	3.69E-04	4.02E-04	4.39E-04	4.77E-04	5.17E-04	5.56E-04	5.98E-04	

Displacement (m)